International Journal of Earth Sciences

U–Pb ages and Hf isotopic composition of zircons in Austrian last glacial loess: constraints on heavy mineral sources and sediment transport pathways

--Manuscript Draft--

Manuscript Number:	IJES-D-14-00245R2
Full Title:	U–Pb ages and Hf isotopic composition of zircons in Austrian last glacial loess: constraints on heavy mineral sources and sediment transport pathways
Article Type:	Original Paper
Keywords:	loess; zircon; U–Pb geochronology; Hf isotope geochemistry; provenance
Corresponding Author:	Gabor Ujvari, Ph.D. MTA Research Centre for Astronomy and Earth Sciences, Geodetic and Geophysical Institute Sopron, HUNGARY
Corresponding Author Secondary Information:	
Corresponding Author's Institution:	MTA Research Centre for Astronomy and Earth Sciences, Geodetic and Geophysical Institute
Corresponding Author's Secondary Institution:	
First Author:	Gabor Ujvari, Ph.D.
First Author Secondary Information:	
Order of Authors:	Gabor Ujvari, Ph.D.
	Urs S Klötzli, Ph.D.
Order of Authors Secondary Information:	
Abstract:	Loess sediments in Austria deposited ca. 30–20 ka ago yield different zircon age signatures for samples collected around Krems (SE Bohemian Massif; samples K23 and S1) and Wels (half-way between the Bohemian Massif and the Eastern Alps; sample A16). CL imaging reveals both old, multi-stage zircons with complex growth histories and inherited cores, and young, first cycle magmatic zircons. Paleoproterozoic ages between 2200 and 1800 Ma (K23 and S1), an age gap of 1800-1000 Ma for S1 and abundant Cadomian grains indicate NW African/North Gondwanan derivation of these zircons. Also A16 yields ages between 630-600 Ma that can be attributed to 'Pan-African' orogenic processes. Significant differences are seen for the <500 Ma part of the age spectra with major age peaks at 493-494 Ma and 344-335 Ma (K23 and S1), and 477 and 287 Ma (A16). All three samples show negative initial εHf signatures (–25 to –10, except one grain with +9.4) implying zircon crystallization from magmas derived by recycling of older continental crust. Hf isotopic compositions of 330-320 Ma old zircons from S1 and K23 preclude a derivation from Bavarian Forest granites and intermediate granitoids. Rather all the data suggest strong contributions of eroded local rocks (South Bohemian pluton, Gföhl unit) to loess material at the SE edge of the Bohemian Massif (K23 and S1), and sourcing of zircons from sediment donor regions in the Eastern Alps for loess at Wels (A16). We tentatively infer primary fluvial transport and secondary aeolian reworking and re-deposition of detritus from western/southwestern directions. Finally, our data highlight that loess zircon ages are fundamentally influenced by fluvial transport, its directions, the interplay of sediment donor regions through the mixing of detritus and zircon fertility of rocks, rather than paleo-wind directions.

Response to reviewers

Reviewer #1: Review of manuscript IJES-D-14-00245R1

The authors did a good job in revising the manuscript according to the reviewers comments. Only a few minor issues still need some attention, as outlined below. After that the manuscript will be ready for publication without further review. *Thank you!*

Line 41: Write "Johnsson 1993" *Corrected.*
Line 71: Replace "CL maps" by "CL images" *Modified.*
Lines 107-108: Write "The last ca. 0.8 million years were characterized by ... " *Corrected.*
Line 118: Check the usage of hyphens, i.e. write "... late- to post-tectonic plutonic rocks ..." *Corrected.*
Line 145: Check the usage of hyphens, i.e. write "... was intruded late– syn- to post-tectonically into the gneisses ..." *Corrected.*
Line 156: Write "Permian– Mesozoic" *Modified.*
Lines 254, 258, 989, 990, and 991: Why are you using "⍰" before the percentage values when you also use "<" and ">" respectively? I suggest deleting "⍰". *All deleted.*
Line 317: Replace "mm" by "µm" *Corrected.*
Line 336: Write "... low- to medium-grade rocks ..." *Amended.*
Lines 492 and 526: I suggest writing "F" in "Formation" with capital letter. *Corrected, also in the caption of Fig. 1.*
Line 726: Delete "e" between "Europe" and "its" *Deleted.*
Line 730: Insert full stop (.) after "histories" *Inserted.*
Line 993: Write "DensityPlotter" without space. *Corrected.*
Line 997: Write "Cadomian/Pan-African" *Corrected.*

Table 3:
- In the interpretation for the Bavarian forest rocks replace "Upper" by "Late" and "Lower" by Early" *Corrected.*
- In the interpretation for the Dobra gneiss replace "protholith" by "protolith" *Corrected.*

U– Pb ages and Hf isotopic composition of zircons in Austrian last glacial loess: constraints on heavy mineral sources and sediment transport pathways

Gábor Újvári[1*], Urs Klötzli[2]

[1]Geodetic and Geophysical Institute, MTA Research Centre for Astronomy and Earth Sciences, H-9400 Sopron, Csatkai E. u. 6-8., Hungary

[2]Department of Lithospheric Research, University of Vienna, Althanstrasse 14, 1090 Vienna, Austria

*Corresponding author: ujvari.gabor@csfk.mta.hu (G. Újvári)

Abstract

Loess sediments in Austria deposited ca. 30– 20 ka ago yield different zircon age signatures for samples collected around Krems (SE Bohemian Massif; samples K23 and S1) and Wels (half-way between the Bohemian Massif and the Eastern Alps; sample A16). CL imaging reveals both old, multi-stage zircons with complex growth histories and inherited cores, and young, first cycle magmatic zircons. Paleoproterozoic ages between 2200 and 1800 Ma (K23 and S1), an age gap of 1800-1000 Ma for S1 and abundant Cadomian grains indicate NW African/North Gondwanan derivation of these zircons. Also A16 yields ages between 630-600 Ma that can be attributed to 'Pan-African' orogenic processes. Significant differences are seen for the <500 Ma part of the age spectra with major age peaks at 493-494 Ma and 344-335 Ma (K23 and S1), and 477 and 287 Ma (A16). All three samples show negative initial ε Hf signatures (– 25 to – 10, except one grain with +9.4) implying zircon crystallization from magmas derived by recycling of older continental crust. Hf isotopic compositions of 330-320 Ma old zircons from S1 and K23 preclude a derivation from Bavarian Forest granites and

intermediate granitoids. Rather all the data suggest strong contributions of eroded local rocks (South Bohemian pluton, Gföhl unit) to loess material at the SE edge of the Bohemian Massif (K23 and S1), and sourcing of zircons from sediment donor regions in the Eastern Alps for loess at Wels (A16). We tentatively infer primary fluvial transport and secondary aeolian reworking and re-deposition of detritus from western/southwestern directions. Finally, our data highlight that loess zircon ages are fundamentally influenced by fluvial transport, its directions, the interplay of sediment donor regions through the mixing of detritus and zircon fertility of rocks, rather than paleo-wind directions.

Keywords: loess; zircon; U– Pb geochronology; Hf isotope geochemistry; provenance

Introduction

Siliciclastic sediments such as wind-blown loess deposits reflect the history of the source terrain from which they were derived and provide insight into sedimentary dispersal systems. Mechanical disaggregation and abrasion, sorting and chemical weathering during erosion, transport and deposition of detritus obscure the rendering of sediment provenance (Johnsson 1993). To minimize these effects refractory minerals such as zircon are widely used in provenance studies (Fedo et al. 2003). What makes zircon a unique provenance proxy is its durability and remarkable chemical stability over a wide range of lithospheric pressures, temperatures, and fluid/melt compositions (Harrison and Watson 1983; Watson and Harrison 1983; Watson 1996; Moecher and Samson 2006), and that, via the U– Pb and Lu– Hf isotopic systems, it provides information on both the timing of thermotectonic history of source terrains and the geochemical environment in which the zircon crystallized (e.g. Patchett et al. 1981; Amelin et al. 2000; Kinny and Maas 2003; Hawkesworth and Kemp, 2006; Scherer et al. 2007; Howard et al. 2009; Weber et al 2012).

Recent loess provenance studies have recognized and demonstrated that single-grain zircon geochronology is more diagnostic in identifying source areas of loess deposits than the bulk mineralogical, elemental, and isotopic approaches (Aleinikoff et al. 1999, 2008; Stevens et al. 2010; Pullen et al. 2011; Újvári et al. 2012; Xiao et al. 2012; Stevens et al. 2013). All of these works, however, have applied the in-situ, single-grain technique without proper characterization of internal structures of zircon grains by high-magnification cathodoluminescence (CL) or backscattered electron (BSE) imaging. It has long been recognized that zircons are variable in external morphology (Pupin 1980), and that internal zonation patterns are of petrogenetic significance (e.g. Hanchar and Miller 1993; Corfu et al. 2003). CL images reveal complex, delicate zonation patterns often reflecting multiple stages of zircon growth and are useful guides of U– Pb measurements. Without detailed CL images, the laser or ion beam could straddle multiple growth zones that may result in mixed ages that are often complicated to interpret (Whitehouse et al. 1999; Hietpas et al. 2011).

In this study, we enhance the quality of in-situ U– Pb age information from single zircons in Austrian loess by mapping their internal structures thereby tapping the full potential of zircon geochronology. Attempts have been made to do this on a quantitative or semi-quantitative basis, i.e. by analyzing a sufficient number of grains (Vermeesch 2004; Andersen 2005), despite the fact that sample preparation and handling have demonstrably larger effects on the reproducibility of zircon age spectra than the number of grains analyzed per sample (Sláma and Košler 2012). To further improve provenance interpretations we aimed at coupling U– Pb ages to Hf isotope geochemistry, again, aided by CL images. The Lu– Hf system in zircon is very resistant to disturbance and it effectively preserves the initial $^{176}Hf/^{177}Hf$ ratio thereby providing a record of Hf isotopic composition of its source environment at the time of crystallization (Kinny and Maas 2003; Scherer et al. 2007). Thus, the Hf isotopic composition of zircon can be utilized as a geochemical tracer of the origin of its host rock and enables to determination of whether crustal samples were formed by melting of the depleted mantle (DM), old crust, or combinations of both (Scherer et al. 2007). In many cases U– Pb age spectra of detrital zircons from different crustal domains are similar and this often obscures provenance interpretations. In such situations combined U– Pb and Hf isotope studies of zircons may allow distinguishing between grains having the same crystallization ages but formed in crustal domains separated from the mantle at different times (Amelin et al. 2000; Scherer et al. 2007).

This analytical approach is here applied to wind-blown loess sediments from the northeastern Alpine foreland in Austria. The sampling strategy focused on collecting coeval loess deposited at around the last glacial maximum (LGM: 19– 26 ka, MIS 2). Two loess sections located east of the southern edge of the Bohemian Massif (BM) (Krems, Stratzing) have been studied together with a third one (Wels) situated on top of a terrace of the Traun-Enns-Plain, half way between the BM and the Eastern Alps (EA). Although previous studies on Moravian loess deposits adjacent to the BM presented evidence for a local source and short distance (50– 100 km) aeolian entrainment for quartz, garnet and zircon grains (Cilek 2001; Lisá 2004; Lisá and Uher 2006; Lisá et al. 2009), we attempted to further constrain the origin of detrital zircons in loess nearby the BM in Austria, track paleo-transport pathways and sediment dispersal patterns.

Here we show that zircons in loess at Krems and Stratzing were likely eroded from local rocks (<10km transport) of the South Bohemian Pluton and Gföhl units, delivered by the Paleo-Danube and subsequently reworked and re-deposited by winds at the sampling sites. Detrital zircons in loess at Wels certainly experienced the same event-sequence, but were derived from Eastern Alpine sources (>50km transport).

Geological setting

Quaternary loess deposits are widespread in the northeastern Alpine foreland along the Danube and its tributaries in Lower and Upper Austria (Fink 1961; van Husen 1981). Loess sedimentation is believed to have commenced in this region from ca. 2.6 Ma, at the turn of the Gauss and Matuyama chrons (Frank et al. 1997) and numerous (at least 17) glacial-interglacial cycles were recorded in the Krems loess-paleosoil sequence after the Olduvai event (from ca. 1.7 Ma) as reported by Fink and Kukla (1977). The last ca. 0.8 million years were characterized by pronounced glacier advances in the EA, as demonstrated by terminal moraines and outwash terraces (Deckenschotter), the remnants of glacial activity (van Husen 2000; Reitner 2007). Glacial grinding has likely been the main mechanism to produce debris in the EA for subsequent loess accumulation in the foreland, while silt production in the BM may be attributable to physical erosion (frost shattering, Cilek 2001) and chemical weathering. The evolution and geological settings of these two possible hinterlands (BM and EA) for loess deposits in Austria are distinct.

Three major tectonic units form the southeast part of the Variscan orogen in Central Europe, of which only the Moldanubian Zone is relevant to our discussion. This comprises the largest part of the southern Bohemian Massif in Austria (Fig. 1). Within this zone a number of different basement series and late- to post-tectonic plutonic rocks can be distinguished mainly based on lithological criteria (Wendt et al. 1994; Petrakakis 1997; Klötzli et al. 1999; Finger et al. 2007). All of the tectono-stratigraphic units are separated from each other by more or less discrete, sub-horizontal shear zones. These are from bottom to top:

The so-called Monotonous Series (Monotone Serie, Ostrong unit) forms the lowermost basement sequence. Major lithologies are masses of monotonous stromatitic to nebulitic gneisses. Subordinate are lenses of orthogneisses, calc-silicate-gneisses and eclogite-amphibolites. Low pressure/high temperature (LP/HT) amphibolite facies metamorphism with cordierite bearing assemblages is typical for this unit.

The granitic to granodioritic 1.38 Ga old Dobra gneiss forms the base of the next higher unit in the east (Gebauer and Friedl 1993), the Varied Series (Bunte Serie, Variegated series, Drosendorf unit). This rather inhomogeneous rock suite is built up by partly migmatitic garnet-sillimanite-biotite-plagioclase gneisses, quartzites, more or less graphite-bearing marbles and calc-silicate rocks, and granitic orthogneisses. Abundant amphibolites closely associated with ultrabasic rocks, marbles, and granitic gneisses (Rehberg and Buschandlwand units) are also present (Petrakakis 1997; Finger et al. 2007).

The next higher units form characteristic klippen on top of the Moldanubian nappe sequence. The so called Gföhl gneiss, a widespread and monotonous alkalifeldspar-rich orthogneiss of granitic composition builds up the lower part of these klippen. Locally transitions to acid granulites can be found (Klötzli et al. 1999; Finger et al. 2007; Friedl et al. 2011).

The highest unit of the Moldanubian Zone is formed by granulites. More massive, less deformed light coloured varieties prevail in the Dunkelstein Wald area, south of the Danube, whereas strongly deformed platy and banded varieties are typical for the St. Leonhard and Blumau occurrences in the north. In the Dunkelsteiner Wald small inclusions of basic granulites and garnet-pyroxenites are also found (Petrakakis 1997; Klötzli et al. 1999; Friedl et al. 2011).

To the west of the Moldanubian basement series large parts of the Moldanubian Zone are occupied by the so-called South Bohemian pluton which was intruded late– syn- to post-tectonically into the gneisses of the Monotonous Series during the Carboniferous. Intrusion ages range from ca. 345 Ma for the oldest plutonites to 300 Ma for the youngest ones (Klötzli et al. 1999; Finger et al. 2007). Ar-Ar cooling ages for hornblende and muscovite suggest high cooling rates and that temperature reached 300 °C before ca. 325 Ma (Dallmeyer et al. 1992).

From top to bottom the Eastern Alps in Austria are made up of 3 major tectonic units (Schmid et al. 2004; Hoinkes et al. 2010):

1. Austroalpine and Southalpine units derived from the Adriatic/Apulian microcontinent
2. Penninic units derived from the Mesozoic Alpine Tethys domain
3. Helvetic and Sub-Penninic units derived from the Variscan European continent and its Permian-Mesozoic cover.

Austoalpine units

The Austroalpine unit forms a complex nappe stack of crustal material which can be subdivided into Lower and Upper Austroalpine units. The Lower Austroalpine unit formed the continental margin towards the Alpine Tethys ocean and was affected by tectonism during the opening and closing of this oceanic realm (Alpine event). It overlies the Penninic Nappes of the Eastern Alps. The Upper Austroalpine unit represents an eo-Alpine nappe pile. Its lowermost unit is the Silvretta-Seckau Nappe system consisting of a basement with a dominating Variscan metamorphic imprint and remnants of Permian-Triassic cover. During the eo-Alpine event it was overprinted by sub-greenschist to greenschist-facies conditions. To the north, the Silvretta-Seckau Nappe system is overlain by the nappes of the Greywacke zone, which consists of greenschist-facies metamorphic Paleozoic sequences, and the nappe system of the Northern Calcareous Alps, comprising unmetamorphosed to lowermost greenschist-facies metamorphic Permian-Mesozoic sediments deposited on the shelf facing originally towards the Meliata ocean. To the south, the Silvretta-Seckau Nappe system is overlain by the Koralpe-Wölz Nappe system which represents an eo-Alpine metamorphic extrusion wedge. The Ötztal-Bundschuh Nappe system shows a similar lithological composition to the Silvretta-Seckau Nappe system, but is positioned on top of the Koralpe-Wölz Nappe system. The overlying Drauzug-Gurktal Nappe system is made up of a Variscan metamorphic basement, anchizonal to greenschist-facies Paleozoic metasedimentary sequences and by unmetamorphosed Permian-Triassic sediments. Within the Ötztal-Bundschuh and Drauzug- Gurktal Nappe systems the eo-Alpine metamorphic grade decreases upwards from amphibolite facies at the base to diagenetic conditions at the top of the nappe pile. The Upper Cretaceous to Paleogene sediments of the Gosau Group represent syn- to postorogenic sediments with respect to the eo-Alpine orogenic event.

Penninic units

The Lower Penninic Nappes consist predominantly of material from the Mesozoic Valais oceanic province and from the northern parts of the joint oceanic basin in the east and make up the central part of the Lower Engadine Window in western Austria. The lower nappes of the mainly Cretaceous Rhenodanubian flysch zone, which are present along the northern margin of the Eastern Alps represent a continuation of the Central Alpine Valais basin sediments into the Eastern Alps. The Glockner Nappe system of the Tauern Window, as well as the nappes of the Rechnitz Window Group, consisting of calcareous flyschoid metasediments and metaophiolites, is thought to be a southern continuation of the lower nappes of the Rhenodanubian flysch zone.

Helvetic and Sub-Penninic units

The European continent consists of a Variscan continental crust, rich in mostly Carboniferous plutonic rocks covered by Carboniferous to Miocene sedimentary sequences. The so-called Sub-Penninic Nappes represent the distal European margin, forming ductilely deformed

Variscan basement and cover nappes. They form the Venediger Nappe system in the Tauern Window.

Eocene to Miocene magmatism

The Periadriatic intrusions comprise calc-alkaline tonalites, granodiorites and granites, and minor alkaline basaltic dykes. They are Eocene to Oligocene in age and related to the break-off of the subducted Alpine Tethys oceanic lithosphere from the distal European margin.

Methods

Sampling, heavy mineral separation and imaging

Loess samples were collected from two loess outcrop located in proximity to the Bohemian Massif at Krems– Wachtberg (sample K23) and Stratzing (sample S1), and from a third section at Wels, (sample A16), situated closer to the Eastern Alps (Fig. 1) (further details in Újvári et al., 2013). All three profiles have previously been dated by ^{14}C or OSL/IRSL (Einwögerer et al. 2009; Preusser and Fiebig 2009; Thiel et al. 2010; Terhorst et al. 2012; Lomax et al. 2014), thereby allowing the sampling of last glacial loess material from all three profiles accumulated around the coldest period of marine isotope stage 2 (MIS 2).

For heavy mineral separation, samples were wet-sieved at 25 and 250 microns under running water, washed in weak acetic acid (5%), then water and acetone and subsequently dried in oven at 50 ºC. Zircon grains were extracted from the bulk sediment using heavy liquid separation and Frantz magnetic separator (Krogh 1982). The grains were then handpicked under the binocular and mounted in epoxy resin. To minimize bias in the age spectra, the morphology and size of the grains were ignored when selecting grains for analysis. It must be admitted, however, that even with a conscious effort to pick representative grains this still introduces a bias towards larger grains, as shown by Sláma and Košler (2012). After polishing, all zircon crystals were cathodoluminescence (CL)-imaged using a FEI Inspect S50 SEM at the Scanning Electron Microscopy and Focused Ion Beam Laboratory, Department of Lithospheric Research, University of Vienna or using a VEGA TESCAN SEM at the Austrian Geological Survey GBA. CL images were subsequently used to classify each zircon crystal into groups with magmatic or metamorphic origin, and also to find the best positions of laser ablation trenches for in situ isotopic analyses.

Mass spectrometry

In situ U– Pb isotopic analyses of detrital zircons were done using a Nu Plasma II multi-collector ICP-MS coupled to a New Wave Research UP-193 solid state laser system at the BigNano Laboratory, Department of Environmental Geosciences, University of Vienna. During the analyses, masses of 238 and 232 were measured in Faraday cups, while masses 208, 207, 206, 204, and 202 were detected in discrete ion counters by using the time resolved protocol of the software package of Nu Instruments. Isotopic measurements were done using a He carrier gas flow of 650 mL min^{-1} and laser settings specified in Table S1 (Supplementary material). Total ablation time varied between 100 and 250 s, including a 30 s gas blank (background) measurement for which the laser shutter remained closed. Repeated measurements of the Plešovice zircon standard (Sláma et al. 2008) were systematically done to correct for laser-induced, depth- and time-dependent elemental fractionation and instrumental mass bias. During the ablation procedure firing of trenches was preferred instead of drilling spots thereby minimizing laser-induced fractionation. Data processing and reduction has been done off-line, using version 3 of LamTool U– Th– Pb (U. Klötzli, unpublished). Raw signal intensities were corrected for IC non-linearity using the method of Richter et al. (2001), and for gas blank based on selection of ‘blank’ and ‘sample’ signal ratio intervals for each measurement. The Pb/U elemental fractionation were corrected for using the ‘intercept method’ of Sylvester and Ghaderi (1997). This correction utilized regression of standard measurements by a quadratic function. ^{204}Hg corrections on mass 204 were made using ^{204}Hg/^{202}Hg=0.2299. No common Pb correction was applied to the data. Zircon U–Pb ages were calculated with Isoplot 3.71 (Ludwig 2008) and plotted as kernel density estimates using DensityPlotter (Vermeesch, 2012), with the ^{206}U/^{238}Pb ages used for zircons dated as <1.0 Ga, and the ^{207}Pb/^{206}Pb series used for grains >1.0 Ga (Nemchin and Cawood 2005). To filter results, zircon ages showing >10% discordance and age uncertainty >10% were rejected. As excessive cutoff severity for discordant ages may compromise the representativeness of the dataset due to selective removal of specific age populations (Nemchin and Cawood 2005; Malusa et al. 2013), a second U–Pb age dataset was established from each loess sample with zircons showing <20% discordance and age uncertainty <20% and both of these datasets are displayed for comparison. This is further justified by the fact that ^{207}Pb/^{206}Pb ages are often unreliable for young grains (e.g. low-U zircons with ages <0.5–0.6 Ga) and therefore useless for calculating discordancy (Nemchin and Cawood 2005; Aleinikoff et al. 2008).

In situ Lu–Hf isotopic analyses of detrital zircons were undertaken using the same Nu Plasma II MC-ICP-MS instrument as for U–Pb geochronology at the University of Vienna and closely followed the procedures described by Klötzli et al. (2009) and Fisher et al. (2011). Laser settings and cup configurations for Lu–Hf are shown in Tables S1 and S2. Each LA-MC-ICP-MS analysis consisted of 30 s of gas background data followed by 100 to 200 s of ablation. Raw ratios from MS intensity data were calculated using the method described by Fietzke et al. (2008). Mass bias effects on Hf were corrected using an exponential law and a ^{179}Hf/^{177}Hf value of 0.7325 for normalization (Kemp et al. 2009). βYb was determined using the measured ^{173}Yb/^{171}Yb and ^{173}Yb/^{171}Yb=1.13269 for normalization (Chu et al., 2002; Fisher et al. 2011). The ^{176}Yb isobaric interference on ^{176}Hf was corrected using the interference-free ^{173}Yb and ^{176}Yb/^{173}Yb was calculated using the measured βYb and the ‘true’

$^{176}Yb/^{173}Yb$ of 0.7962 (Chu et al., 2002; Fisher et al. 2011). The ^{176}Lu isobaric interference on ^{176}Hf was determined using the measured, interference-free mass ^{175}Lu, setting $\beta Lu=\beta Yb$ and using the 'true' $^{176}Lu/^{175}Lu$ of 0.026549 (Vervoort et al. 2004; Kemp et al. 2009; Fisher et al. 2011). The calculated ^{176}Lu and ^{176}Yb intensities on the total 176 signal were subtracted, the remaining mass 176 signal is taken as solely being ^{176}Hf and the interference-corrected $^{176}Hf/^{177}Hf$ was calculated thereof. The $^{176}Lu/^{177}Hf$ and $^{176}Yb/^{177}Hf$ were corrected for mass bias using βHf.

Outlier rejection of the $^{176}Hf/^{177}Hf$ for each analysis was done using a two-standard deviation criterion, while no outlier rejections were performed for $^{176}Lu/^{177}Hf$ and $^{176}Yb/^{177}Hf$ as these ratios often vary considerably in both synthetic and natural zircon crystals (Fisher et al. 2011). Additionally, the very small signal intensities on Lu and Hf resulted in comparably large errors.

Reported errors are two standard errors of the mean (2SE). As analytical errors on single measurements are significantly larger than the overall reproducibility of the Mud Tank MM– 1 reference zircon the overall uncertainty of this latter was not propagated into the final errors. The Mud Tank MM– 1 zircon was used as external standard to determine overall uncertainties and accuracy. During the course of this study 39 measurements were made on Mud Tank MM– 1 (dimensions: 20 µm diameter and 200 µm length) and 37 out of 39 measurements give the following mean values: $^{176}Hf/^{177}Hf=0.28250\pm0.00002$ (0.006%), $^{176}Lu/^{177}Hf=0.00005\pm0.00004$ (76%), and $^{176}Yb/^{177}Hf=0.00177\pm0.00209$ (118%). The remaining two measurements yielded too low $^{176}Hf/^{177}Hf$ and were not taken into account. The mean $^{176}Hf/^{177}Hf$ ratio given above is within error identical to the recommended values reported by Woodhead and Hergt (2005), Griffin et al. (2006), and Kemp et al. (2009) for laser ablation analysis. This demonstrates that the experimental setup allows for valid ^{176}Lu and ^{176}Yb corrections and results in reliable zircon $^{176}Hf/^{177}Hf$ ratios.

Present-day ε Hf values (ε Hf_0) have been calculated using the new chondritic Hf data of $^{176}Hf/^{177}Hf_{CHUR-0}$=0.282785±0.000011 (Bouvier et al. 2008), and a ^{176}Lu decay constant of $\lambda^{176}Lu=1.867\pm0.008\times10^{-11}$ a^{-1} (Söderlund et al. 2004) has been used to calculate initial $^{176}Hf/^{177}Hf$ ratios (i.e. $^{176}Hf/^{177}Hf$ at the time *t* of zircon crystallization; $^{176}Hf/^{177}Hf_t$). A chondritic Lu/Hf value of $^{176}Lu/^{177}Hf_{CHUR-0}$=0.0336±0.0001 (Bouvier et al. 2008) has been applied in all ε Hf_t calculations. Two-stage crustal residence ages (τ^c_{DM}– Hf) have been calculated using the initial $^{176}Hf/^{177}Hf$ values of each zircon ($^{176}Hf/^{177}Hf_t$), an assumed average crustal $^{176}Lu/^{177}Hf$ of 0.015 (Griffin et al. 2004; Condie et al. 2005), and a depleted mantle model with $^{176}Hf/^{177}Hf_{DM}$=0.283224 (Vervoort et al. 2000) and $^{176}Lu/^{177}Hf_{DM}$=0.03836 (calculated for εHf=0 at 4500 Ma; Weber et al. 2012). Such two-stage model ages provide a qualitative estimate of the time of separation of the zircon's host rock from a hypothetical depleted mantle reservoir and have successfully been used in some previous zircon provenance studies (e.g. Bodet and Schärer 2000; Griffin et al. 2004; Augustsson et al. 2006; Bahlburg et al. 2009, 2010).

Results

The analyzed loess samples contain various heavy minerals. Zircon grains are present in all three samples, but those found in sample A16 at Wels are generally smaller in size (mostly around and below 100 µm), while larger crystals (130– 200 µm) appear frequently in the other two (K23 and S1, Krems and Stratzing; referred to as samples at Krems hereafter). Zircons were colorless and many different forms could be distinguished from less frequent euhedral to more frequent sub-rounded (sometimes rounded) crystals and prismatic and anhedral fragments. Elongated prismatic forms appear exclusively in loess samples at Krems, Bohemian Massif (K23 and S1). Unlike zircon, sphene (titanite) was only found in loess samples at Krems (K23 and S1). These grains, which were subsequently checked by SEM-

EDX for their chemical compositions, are mostly colorless, sometimes slightly honey yellow and rounded/ sub-rounded. While apatite is present in all three samples (usually colorless, stubby forms, sometimes reddish-brown), another phosphate heavy mineral monazite appears in samples at Krems (K23 and S1). These are pale yellow and almost colorless with some yellowish-brown stain, and have rounded, egg-shaped forms. Likewise apatite, chlorite and garnet are constituents of all three loess samples, but an extraordinary number of garnets were found in loess samples around Krems (Bohemian Massif). The vast majority of these garnets are euhedral crystals with pink color. Both staurolite and sillimanite, and also remarkable amounts of brown to reddish-brown biotite are present in these loess samples (K23 and S1). The metamorphic index minerals (e.g. staurolite and sillimanite) with garnet are indicative of a metamorphic hinterland with medium to high-grade metamorphic rocks for loess samples at Krems (BM). As for the sample at Wels (A16), the heavy mineral assemblage (e.g. chlorite, garnet) implies contributions from low- to medium-grade rocks to loess at this site. Neither kyanite nor Cr-spinel have been found in the samples which would refer to high-P metamorphic rocks or oceanic crust in the hinterland, but it must be emphasized that the heavy mineral analyses cannot be regarded as detailed, in-depth studies.

Altogether 86, 51 and 45 zircon grains have been CL-imaged and subsequently U‒ Pb dated from loess samples S1, K23 and A16 (note that not all of these U‒ Pb ages have been used for creating the U‒ Pb age spectra due to data filtering specified in the ‘Methods’ section). Most of them (46 to 64%) are magmatic in origin (40 in S1, 33 in K23 and 27 in A16) and 14 to 23.5% of these crystals are interpreted as having been eroded from metamorphic rocks (12 in S1, 12 in K23 and 7 in A16). Some representative magmatic and metamorphic crystals, also with recrystallization rims and grains with inherited cores are displayed in Figs. 2 and 3. The rest of the zircon grains could not unambiguously be classified into any of these two groups.

Before analyzing U– Pb age spectra it is crucial to evaluate how representative these dates are and what is the likelihood of missing age populations crucial for provenance interpretation. Table 1 provides information on this and is based on the binomial probability formulation by Andersen (2005), which we prefer over that of Vermeesch (2004). While the number of grains analyzed in S1 (and K23 depending on concordance criteria) seems appropriate, this issue becomes critical in sample A16 where the failure rate to detect an age population with an abundance X_i=10% reaches 22.9 to 53.1 percent (Table 1). At the same time, if an age population was detected in A16 (within the 90-110% concordance criteria) and this population was not found in the other two samples (S1 and K23) then this can be regarded as a basic diagnostic feature. We will see below that this is exactly the case.

U– Pb age spectra of samples at Krems (S1 and K23) show a similar distribution of ages (Fig. 4, Tables S3-4 as Supplementary material) with major age peaks at 493-494 and 335-344 Ma. The majority of these grains are magmatic in origin. A striking feature of S1 is the absence of ages between 1700-800 Ma, while this age window is narrower (1200-750 Ma) for K23. Considering the relatively low detection limits for S1 (Table 1), this age gap seems to be a real one. In contrast to samples at Krems (S1 and K23), the prominent age maximum of the age distribution lies at 287 Ma for the sample at Wels (A16), and also some ages are observed at 450 and 600 Ma, up to 1500 Ma.

Lu– Hf isotopic compositions of 30, 14 and 10 grains have been analyzed from samples S1, K23 and A16, but only 18, 6 and 4 grains provided both useful U– Pb ages and Lu– Hf isotopic compositions (Table 2). With the exception of three grains, all have $^{176}Lu/^{177}Hf$ ratios below 0.0019 and numerous zircons have lower than 0.001. Present-day $^{176}Hf/^{177}Hf$ ratios range between 0.281941 and 0.282191, corresponding to present day ε Hf values of – 29.8 to – 21. Initial $^{176}Hf/^{177}Hf$ ratios and ε Hf values vary between 0.281933 and 0.282185, and – 24.7 to 9.4, with most of the grains yielding ε Hf_t values between – 22.2 and – 10.9. Two-stage crustal residence ages (τ^{c}_{DM}– Hf) range from ~2000 to 2700 Ma for all three loess samples. Only one zircon yields a comparatively younger model age of 1712 Ma from the sample at Wels (A16; Table 2).

Discussion

Interpretation of the zircon U– Pb age and Hf isotopic record

The oldest detrital zircon ^{207}Pb/^{206}Pb age from the sample at Wels (A16) is 1657±102 Ma. This grain has an initial ε Hf value of 9.4 demonstrating its derivation from juvenile, mantle-derived sources (Table 2 and Fig. 5). In contrast to the sample at Wels (A16), loess sediments at Krems (S1 and K23) yield more zircons with Paleoproterozoic ages ranging mostly between 2200 and 1800 Ma (Fig. 4 and Supplementary Tables S3– 5), which are typical of the western part of the West African craton (Linnemann et al. 2008). Most of these grains are magmatic and can possibly link with plutonic events of the Eburnean orogeny (Egal et al. 2002). A striking feature of the age distribution of loess zircons at Krems (sample S1) is the lack of ages between 1750 and 750 Ma. This Late Paleoproterozoic– Mesoproterozoic age gap (1800– 1000 Ma) is characteristic for rocks of the Moldanubian unit (Friedl et al. 2004; Košler et al. 2014) and also demonstrates NW African/North Gondwanan derivation of Armorican type terranes (Tait et al. 1997; Samson et al. 2005; Gerdes and Zeh 2006; Meinhold et al. 2011, 2013). At the same time, some zircon ages for sample K23 (Krems) are found between 1650 and 1200– 1100 Ma and this holds true for sample A16. All three samples provide Late Neoproterozoic zircon ages at around 630 to 600 Ma that are attributable to ‘Pan– African’ orogenic processes (Linnemann et al. 2008), and samples at Krems (S1 and K23) are rich in Cadomian grains (590-550 Ma), represented by age clusters at ~580-590 Ma (Fig. 4a and b). These Cadomian ages again carry evidence of peri-Gondwanan origin of the basement blocks the zircons originated from (Stampfli et al. 2002). A peculiar feature of zircon age distributions of samples at Krems (S1 and K23) is the dominant age populations at ~490 Ma. Both metamorphic and magmatic grains of Cambrian-Ordovician age are found in these two samples. Evidence for intensive magmatic activity of this age has been presented by Friedl et al. (2004) from the Gföhl gneiss zircons (Table 3), a unit that is closely located to the sampling sites and drained by the River Danube. Initial ε Hf values between − 10 and − 20 of these 630 to 470 Ma old grains imply zircon crystallization from magmas derived by recycling of older continental crust for all three samples. Hf isotopic compositions of Cadomian magmatic zircons (590-560 Ma) from samples at Krems (S1 and K23) point to a possible derivation of these grains from a Cadomian magmatic arc (Linnemann et al. 2008). The negative initial ε Hf values (− 19 to − 10) of the 490 Ma age group reveal that the (re)crystallization of these grains can possibly related to a somewhat nebulous intra-Rheic subduction zone with a not too evolved volcanic arc and the involvement of continental crust.

U− Pb age distributions of detrital zircons in samples at Krems (S1 and K23) display prominent age peaks at 335 and 344 Ma (Variscan events), while the sample at Wels (A16) shows a younger one at 287 Ma. Characteristic for S1 and K23 (Krems) are the relatively low number of metamorphic zircons, most of them with ages of 380 to 340 Ma. These zircons are records of different stages of the Variscan metamorphic overprints of Moldanubian rocks in the BM lasted from ~380− 370 to 340− 335 Ma (Petrakakis 1997; Friedl et al. 2011; Table 3). However, the majority of Late Devonian/Carboniferous zircons in samples at Krems (S1 and K23) are magmatic in origin with ages ranging from~370 to 320 Ma (Fig. 3). Most of these zircons form an age group of 350− 330 Ma, and only few ages fall between 330 and 320 Ma. Granite emplacements during the Variscan plutonism in the South Bohemian batholith were dated to 350 to 320 Ma (e.g. Klötzli and Parrish 1996; Klötzli et al. 2001; Gerdes et al. 2003; Finger et al. 2007; and Table 3) and our detrital zircon age data suggest a strong contribution from these sources. Former observations by Gerdes et al. (1996) and Klötzli et al. (2001) that the granitoids of the South Bohemian pluton show no pronounced mantle signatures and the melts were essentially produced through anatectic recycling of older, presumably Cadomian, continental crust is further corroborated by the Hf isotope signatures (ε Hf_t from – 22.2 to – 13.7) of the detrital zircons of 350– 320 Ma age (Figs. 3 and 5). Also these low initial ε Hf values and calculated two-stage crustal residence ages (τ^{c}_{DM}– Hf) of 2650 to 2100 Ma preclude a derivation of loess detrital zircons at Krems (S1 and K23) from Bavarian Forest granites and intermediate granitoids having similar ages (334 to 315 Ma), but more radiogenic Hf isotopic compositions and much younger model ages (ε Hf_t from – 5.6 to – 0.4, τ^{c}_{DM}– Hf: 1480 to 1200 Ma; Siebel and Chen 2010; Table 3).

As mentioned above, the sample at Wels (A16) differs from those at Krems (S1 and K23) as two magmatic zircons with ages of 296±6 and 282±17 Ma are present in sample A16, while these Late Carboniferous/Permian grains are completely missing in the other two samples at Krems (S1 and K23). Considering that this youngest age population is represented by two zircons (296±6 and 282±17 Ma) out of the 6 highly concordant ages of sample A16 and supposing that sample A16 is representative of its source, this population may be safely assumed to be an important constituent of the sediment and the probability of finding it equals to 2/6=1/3. From this we calculate that the probability of overlooking this age population is $p_{n_i=0} = 1 - \frac{1}{3} = 2/3$. Rearranging the equation of $p_{n_i=0} = (1 - X_i)^n$ that gives the binomial probability of overlooking an age population with an abundance X_i in the sediment (see Andersen 2005, Eq. 2a), we get that *Xi*, the relative abundance of the *i*th population, is $X_i = 1 - \sqrt[n]{p_{n_i=0}} = 1 - (p_{n_i=0})^{1/n}$, where *n* is the number of zircons having concordant, i.e. useful ages. Applying this to the youngest population in sample A16 at Wels represented by ages of 296±6 and 282±17 Ma, we get the crude estimation of 6.5% for the relative abundance of this population. Knowing that pL=0.5 marks an upper abundance limit for populations that are more probably overlooked than observed in *n* analyses (Andersen 2005) and that these values range between 1.4 to 4.0% for samples at Krems (S1 and K23; Table 1), it is clear that this youngest population should have been found in samples at Krems (S1 and K23) if they were present in their hinterland. Based partly on the above considerations and figures we argue for an Eastern Alpine affinity and derivation of zircons in sample A16 at Wels. At the same time, there is little doubt that zircons in the other two samples at Krems (S1 and K23) were eroded from exposed granitic and various metamorphic rocks of the south BM in the vicinity of the sampling sites (e.g. South Bohemian pluton, Gföhl unit).

Implications for paleo‒ transport modes and routes

Heavy minerals like zircon constitute only minor parts of loess material, so they are likely not fully representative of the whole rock. Physical laws define that these minerals of mostly 50 to 150‒ 200 µm in size in loess are transported in saltation by wind and the transport is short‒ term (Tsoar and Pye 1987; Újvári et al. 2013). This holds true even if large (>75 µm) quartz grains are transported for long distances (several thousands of kilometers) in some rare cases (Betzer et al. 1998). Whole rock geochemical and Sr‒ Nd isotopic data and zircon age patterns demonstrate the basic role of fluvial entrainment of minerals in loess formation (Gallet et al 1998; Buggle et al. 2008; Újvári et al. 2008; Újvári et al. 2012; Stevens et al. 2013) as hypothesized by Smalley et al. (2009). Here we argue for a two-stage model, an initial fluvial and subsequent aeolian transport of heavy minerals in Austrian loess, as proposed for rutiles by Újvári et al. (2013). While the possibility of direct aeolian deflation of the in-situ weathering products of rocks from sparsely vegetated surfaces cannot be dismissed, this scenario seems less likely based on the physical mechanisms of wind erosion and emission of mineral particles (Shao 2009). Also fluvial activity is needed to periodically destroy surface crusts of alluvial material, which may hinder or at least very strongly subdue wind deflation (Pye 1995; Shao 2009).

Our zircon U– Pb age and Hf isotopic data point to significant contributions of heavy minerals from eroded local rocks to loess in Austria. This is consistent with inferences made by Újvári et al. (2013) who found that local metamorphic sources may have released the majority of detrital rutiles recovered from loess samples in Austria. Recent studies of modern river systems demonstrate that detrital zircon age populations are heavily influenced by local bedrock and the influx of feeder tributaries, and the continued input of detritus along rivers causes progressive masking of upstream sources (Cawood et al 2003; Hietpas et al 2011). This may be an explanation why the detrital zircon signal of Bavarian Forest granitoids are not seen in our samples as unraveled by the Hf isotopic compositions and crustal model ages of 330-320 Ma old zircons in samples at Krems (S1 and K23). Both the new zircon U– Pb and Hf isotope data (this study) and the published rutile chemistry and U– Pb age data (Újvári et al. 2013) confirm the derivation of detritus from the Eastern Alps for the sample at Wels (A16), and again, highlight the importance of fluvial entrainment. Here, in lack of any zircon or rutile data, we cannot exclude the Rhenohercynian flysch as a sediment donor region, but it is more than clear that any N– S material transport from the western BM to the region of Wels (A16) can be excluded. This is supported by paleo-circulation models for the region, too (Florineth and Schlüchter 2000; Renssen et al. 2007). Similarly, recycling of loess zircons at Krems (S1 and K23) from the coarse-grained clastic fluvial to deltaic sediments of the Upper Miocene Hollabrunn-Mistelbach Formation (NE of the sampling sites, Fig. 1) seems also a viable alternative. These fluvial sediments were eroded by the proto-Danube from rocks of the SE part of the BM (Nehyba and Roetzel, 2004). Thus zircon age patterns resembling those of loess samples (S1 and K23) are expected from these fluvial sediments and also all of their heavy mineral spectra are garnet dominated (Brunnacker et al. 1979), similarly to S1 and K23 loess samples at Krems. Together with this, neither the appearance of euhedral zircons in the studied loess samples (S1 and K23) nor the modeled paleo-wind directions favor this recycling scenario.

Here, we have to underline that any inferences on paleo– wind directions from loess heavy mineral signals remain hypothetic and weakly supported in the light of the physics of transport and deposition. Rather what is seen in loess zircon ages are more profoundly influenced by fluvial transport, its directions, the interplay of sediment donor regions through the mixing of detritus and zircon fertility of rocks in the drainage basin (Moecher and Samson 2006; Dickinson 2008). In a broader context, these observations have important implications for heavy mineral sources in loess of the Chinese Loess Plateau where debates on Tibetan Plateau versus desert provenance of loess (and heavy minerals in it) are still unsettled (Pullen et al. 2011; Xiao et al. 2012; Stevens et al. 2013). In any case, our findings regarding the crucial role of fluvial processes in defining heavy mineral compositions in Austrian loess and the two-stage model correspond with the ideas of Stevens et al. (2013) who suggested a genetic linkage between the Yellow river sediments, originating in the Tibetan Plateau, and loess on the Chinese Loess Plateau.

Summary and conclusions

U– Pb geochronology and Hf isotope geochemistry of CL-mapped detrital zircon crystals from late glacial loess deposits in Austria reveal proximal BM sources (South Bohemian pluton, Gföhl unit) of these minerals from samples at Krems and Stratzing (K23, S1) and exclude a derivation of 330-320 Ma old zircons from Bavarian Forest granitoids. This latter finding corroborates the significance and strong influence of immediate source areas (with transport distances less than 10 km) on heavy mineral compositions of loess at Krems and Stratzing. This can be explained by a primary fluvial entrainment of heavy minerals in the course of which the local input of zircons result in progressive downstream dilution and masking of upstream zircon signatures. Aeolian reworking of this fluvial material in proximal depocenters is thought to be responsible for the final transport and deposition of particles making up loess sediments around Krems. This event-sequence likely holds true even if the clastic sediments of the nearby Hollabrunn-Mistelbach Formation had eventually acted as an immediate source, since the ultimate source of heavy minerals in these fluvial sediments are also igneous and metamorphic rocks of the southeast BM.

A similar erosion-deposition history of zircons in loess at Wels (A16) is proposed but with sediment donor regions in the Eastern Alps (with transport distances more than 50 km). This inference is largely based on zircon age spectra with different peaks at 295 and 465 Ma in contrast to 350-335 and 490-500 Ma for loess at around Krems. These findings also allow some inferences to be made over depositional wind regimes operating in this region during the last glacial maximum. A significant proportion of storms appear to have tracked from the west, as with the regime for the LGM modeled in larger-scale simulations, and a north to south transport seems very unlikely based on zircon age signatures of sample A16 from Wels. It must be emphasized, however, that the compositions and ages of loess heavy minerals, including zircon and rutile is profoundly determined by mixing of detritus from various sediment donor regions during fluvial transport and the fertility of rocks on these terrains, thus any inferences on major aeolian transport pathways can be considered only hypothetical.

Acknowledgements

This research was supported through a postdoc fellowship to GÚ provided by the Stipendiumstiftung der Republik Österreich (ICM-2010-00919, ICM-2010-03401) and the Bolyai János Research Scholarship of the Hungarian Academy of Sciences (GÚ). The authors are especially grateful to Christine Neugebauer-Maresch and her research group at the

Academy of Science of Austria, as well as Markus Fiebig and Franz Ottner for providing samples and help with the field work. Insightful and constructive comments made by the two reviewers (G Meinhold and T Stevens) improved this paper substantially. Editorial handling by W-C Dullo is greatfully acknowledged.

Appendix

Uncertainty propagation for $^{176}Hf/^{177}Hf_{t,\ zircon}$ (or initial $^{176}Hf/^{177}Hf_{zircon}$)

The $^{176}Hf/^{177}Hf$ composition of zircon at the time of crystallization (i.e. initial $^{176}Hf/^{177}Hf_{zircon}$ or $^{176}Hf/^{177}Hf_{t,zircon}$) is calculated as

$$D_t = D_m - P_m(e^{\lambda t} - 1) \tag{A.1}$$

, where D_t=$^{176}Hf/^{177}Hf_{t,zircon}$, D_m=$^{176}Hf/^{177}Hf_{zircon\text{-}measured}$, P_m=$^{176}Lu/^{177}Hf_{zircon\text{-}measured}$, $\lambda=\lambda_{176Lu}=1.867\pm0.008\times10^{-11}\ a^{-1}$ (Söderlund et al. 2004) and t is the crystallization age of zircon.

Using the law of propagation of uncertainty, the combined standard uncertainty for D_t is given by

$$\sigma_{D_t}^2 = \left(\frac{\partial D_t}{\partial D_m}\sigma_{D_m}\right)^2 + \left(\frac{\partial D_t}{\partial P_m}\sigma_{P_m}\right)^2 + \left(\frac{\partial D_t}{\partial \lambda}\sigma_{\lambda}\right)^2 + \left(\frac{\partial D_t}{\partial t}\sigma_{t}\right)^2 \tag{A.2}$$

Since

$$\frac{\partial D_t}{\partial D_m} = 1 \tag{A.3}$$

$$\frac{\partial D_t}{\partial P_m} = e^{\lambda t} - 1 \tag{A.4}$$

$$\frac{\partial D_t}{\partial \lambda} = (e^{\lambda t} - 1)P_m t \tag{A.5}$$

$$\frac{\partial D_t}{\partial t} = (e^{\lambda t} - 1)P_m \lambda \tag{A.6}$$

the combined uncertainty of D_t=$^{176}Hf/^{177}Hf_{t,zircon}$ is

$$\sigma_{D_t} = \sqrt{\sigma_{D_m}^2 + \left((e^{\lambda t} - 1)\sigma_{P_m}\right)^2 + ((e^{\lambda t} - 1)P_m t \sigma_\lambda)^2 + ((e^{\lambda t} - 1)P_m \lambda \sigma_t)^2} \quad \text{(A.7)}$$

References

Aleinikoff JN, Muhs DR, Sauer RR, Fanning CM (1999) Late Quaternary loess in northeastern Colorado, II: Pb isotopic evidence for the variability of loess sources. Geological Society of America Bulletin 111:1876– 1883.

Aleinikoff JN, Muhs DR, Bettis III EA, Johnson WC, Fanning CM, Benton R (2008) Isotopic evidence for the diversity of late Quaternary loess in Nebraska: glaciogenic and nonglaciogenic sources. Geological Society of America Bulletin 120:1362–1377.

Amelin YV, Lee DC, Halliday AN (2000) Early–middle Archaean crustal evolution deduced from Lu–Hf and U–Pb isotopic studies of single zircon grains. Geochimica et Cosmochimica Acta 64:4205–4225.

Andersen T (2005) Detrital zircons as tracers of sedimentary provenance: limiting conditions from statistics and numerical simulation. Chemical Geology 216:249–270.

Augustsson C, Münker M, Bahlburg H, Fanning CM (2006) Provenance of Late Palaeozoic metasediments of the SW South American Gondwana margin from combined U–Pb ages and Hf isotope compositions of single detrital zircons. Journal of the Geological Society, London 163:983–995.

Bahlburg H, Vervoort JD, Du Frane SA, Bock B, Augustsson C, Reimann C (2009) Timing of crust formation and recycling in accretionary orogens: Insights learned from the western margin of South America. Earth-Science Reviews 97:215– 241.

Bahlburg H, Vervoort JD, Du Frane SA (2010) Plate tectonic significance of Middle Cambrian and Ordovician siliciclastic rocks of the Bavarian Facies, Armorican Terrane Assemblage, Germany — U–Pb and Hf isotope evidence from detrital zircons. Gondwana Research 17:223–235.

Beck‒ Mannagetta P (1964) Geologische Übersichtskarte der Republik Österreich. Geologische Bundesanstalt, Wien.

Betzer PR, Carder KL, Duce RA, Merrill JT, Tindale NW, Uematsu M, Costello DK, Young RW, Feely RA, Breland JA, Bernstein RE, Greco AM (1988) Long‒ range transport of giant mineral aerosol particles. Nature 336:568‒ 571.

Bodet F, Schärer U (2000) Evolution of the SE-Asian continent from U-Pb and Hf isotopes in single grains of zircon and baddeleyite from large rivers. Geochimica et Cosmochimica Acta 64:2067–2091.

Bouvier A, Vervoort JD, Patchett PJ (2008) The Lu–Hf and Sm–Nd isotopic composition of CHUR: constraints from unequilibrated chondrites and implications for the bulk composition of terrestrial planets. Earth and Planetary Science Letters 273:48–57.

Brunnacker K, Fink J, Razirad M, Tillmanns W (1979) Der Hollabrunner Schotter östlich von Krems, Niederösterreich. Zeitschrift der Deutschen Geologischen Gesellschaft 130:303–322.

Buggle B, Glaser B, Zöller L, Hambach U, Markovic S, Glaser I, Gerasimenko N (2008) Geochemical characterization and origin of Southeastern and Eastern European loesses (Serbia, Romania, Ukraine). Quaternary Science Reviews 27:1058‒ 1075.

Cawood P, Nemchin A, Freeman M, Sircombe K (2003) Linking source and sedimentary basin: Detrital zircon record of sediment flux along a modern river system and implications for provenance studies. Earth and Planetary Science Letters 210:259–268.

Cesare B, Rubatto D, Hermann J, Barzi L (2002) Evidence for Late Carboniferous subduction type magmatism in mafic–ultramafic cumulates of the SW Tauern window (Eastern Alps). Contributions to Mineralogy and Petrology 142:449–464

Chu NC, Taylor RN, Chavagnac V, Nesbitt RW, Boella RM, Milton JA, German CR, Bayon G, Burton K (2002) Hf isotope ratio analysis using multi-collector inductively coupled plasma mass spectrometry: an evaluation of isobaric interference corrections. Journal of Analytical Atomic Spectrometry 17:1567–1574.

Cilek V (2001) The loess deposits of the Bohemian Massif: silt provenance, palaeometeorology and loessification processes. Quaternary International 76/77:123–128.

Condie KC, Beyer E, Belousova EA, Griffin WL, O'Reilly SY (2005) U–Pb isotopic ages and Hf isotopic composition of single zircons: the search for juvenile Precambrian continental crust. Precambrian Research 139:42–100.

Corfu F, Hanchar JM, Hoskin PWO, Kinny P (2003) Atlas of zircon textures. In: Hanchar JM, Hoskin PWO (eds) Zircon, Reviews in Mineralogy and Geochemistry 53, pp 469–500.

Dallmeyer RD, Neubauer F, Höck V (1992) Chronology of late Paleozoic tectonothermal activity in the southeastern Bohemian Massiv, Austria (Moldanubian and Moravo–Silesian zones): $^{40}Ar/^{39}Ar$ mineral age controls. Tectonophysics 210:135–153.

Dickinson W (2008) Impact of differential zircon fertility of granitoid basement rocks in North America on age populations of detrital zircons and implications for granite petrogenesis. Earth and Planetary Science Letters 275:80–92.

Egal E, Thiéblemont D, Lahondère D, Guerrot C, Costea CA, Iliescu D, Delor C, Goujou J-C, Lafon JM, Tegyey M, Diaby S, Kolié P (2002) Late Eburnean granitization and tectonics along the western and northwestern margin of the Archean Kénéma–Man domain (Guinea, West African Craton). Precambrian Research 117:57–84.

Eichhorn R, Höll R, Loth G, Kennedy A (1999) Implications of U–Pb SHRIMP zircon data on the age and evolution of the Felbertal tungsten deposit (Tauern Window, Austria). International Journal of Earth Sciences 88:496–512.

Eichhorn R, Loth G, Höll R, Finger F, Schermaier A, Kennedy A (2000) Multistage Variscan magmatism in the Tauern Window (Austria) unveiled by U/Pb SHRIMP zircon data. Contributions to Mineralogy and Petrology 139:418–435.

Eichhorn R, Loth G, Kennedy A (2001) Unravelling the pre-Variscan evolution of the Habach terrane (Tauern Window, Austria) by U–Pb SHRIMP zircon data. Contributions to Mineralogy and Petrology 142:147–162.

Einwögerer T, Händel M, Neugebauer-Maresch C, Simon U, Steier P, Teschler-Nicola M, Wild EM (2009). ^{14}C dating of the Upper Paleolithic site at Krems-Wachtberg, Austria. Radiocarbon 51:847– 855.

Fedo CM, Sircombe KN, Rainbird RH (2003) Detrital zircon analysis of the sedimentary record. In: Hanchar JM, Hoskin PWO (eds) Zircon, Reviews in Mineralogy and Geochemistry 53, pp 277– 303.

Fisher CM, Hanchar JM, Samson SD, Dhuime B, Blichert-Toft J, Vervoort JD, Lam R (2011) Synthetic zircon doped with hafnium and rare earth elements: A reference material for in situ hafnium isotope analysis. Chemical Geology 286:32–47.

Fietzke J, Liebetrau V, Günther D, Gürs K, Hametner K, Zumholz K, Hansteen TH, Eisenhauer A (2008) An alternative data acquisition and evaluation strategy for improved isotope ratio precision using LA-MC-ICP-MS applied to stable and radiogenic strontium isotopes in carbonates. Journal of Analytical Atomic Spectrometry 23:955–961.

Finger F, Gerdes A, Janoušek V, René M, Riegler G (2007) Resolving the Variscan evolution of the Moldanubian sector of the Bohemian Massif: the significance of the Bavarian and the Moravo-Moldanubian tectonometamorphic phases. Journal of Geosciences 52:9–28.

Fink J (1961) Die Gliederung des Jungpleistozäns in Österreich. Mitteilungen der Geologischen Gesellschaft 54:1–25.

Fink J, Kukla GJ (1977) Pleistocene climates in Central Europe: At least 17 interglacials after the Olduvai Event. Quaternary Research 7:363–371.

Florineth D, Schlüchter Ch (2000) Alpine evidence for atmospheric circulation patterns in Europe during the Last Glacial Maximum. Quaternary Research 54:295– 308.

Frank Ch, Nagel D, Rabeder G (1997) Chronologie des österreichischen Plio-Pleistozäns. In: Döppes D, Rabeder G (eds) Pliozäne und pleistozäne Faunen Österreichs, pp 359–374.

Friedl G, Finger F, Paquette J-L, von Quadt A, McNaughton NJ, Fletcher IR (2004) Pre-Variscan geological events in the Austrian part of the Bohemian Massif deduced from U– Pb zircon ages. International Journal of Earth Sciences 93:802– 823.

Friedl G, Cooke RA, Finger F, McNaughton NJ, Fletcher IR (2011) Timing of Variscan HP-HT metamorphism in the Moldanubian Zone of the Bohemian Massif: U– Pb SHRIMP dating on multiply zoned zircons from a granulite from the Dunkelsteiner Wald Massif, Lower Austria. Mineralogy and Petrology 102:63–75.

Gallet S, Jahn B, Van Vliet Lanoë B, Dia A, Rossello E (1998) Loess geochemistry and its implications for particle origin and composition of the upper continental crust. Earth and Planetary Science Letters 156:157–172.

Gebauer D, Friedl G (1993) A 1.38 Ga protolith age for the Dobra orthogneiss (Moldanubian zone of the southern Bohemian massif, NE-Austria): evidence from ion-microprobe (SHRIMP)-dating of zircon. European Journal of Mineralogy 5:115.

Gerdes A, Zeh A (2006) Combined U–Pb and Hf isotope LA-(MC-)ICP-MS analyses of detrital zircons; comparison with SHRIMP and new constraints for the provenance and age of an Armorican metasediment in central Germany. Earth and Planetary Science Letters 249:47–61.

Gerdes A, Wörner G, Finger F (1996) Mantle sources in Hercynian granitoids? A trace element and isotope study. Journal of Conference Abstracts 1:201.

Gerdes A, Friedl G, Parrish RR, Finger F (2003) High-resolution geochronology of Variscan granite emplacement – the South Bohemian Batholith. Journal of the Czech Geological Society 48: 53–54.

Griffin WL, Belousova EA, Shee SR, Pearson NJ, O'Reilly SY (2004) Archean crustal evolution in the northern Yilgarn Craton: U–Pb and Hf-isotope evidence from detrital zircons. Precambrian Research 131:231–282.

Griffin WL, Pearson NJ, Belousova EA, Saeed A (2006) Comment: Hf-isotope heterogeneity in zircon 91500. Chemical Geology 233:358–363.

Haase D, Fink J, Haase G, Ruske R, Pecsi M, Richter H, Altermann M, Jäger KD (2007) Loess in Europe – its spatial distribution based on a European Loess Map, scale 1:2,500,000. Quaternary Science Reviews 26:1301– 1312.

Hanchar JM, Miller CF (1993) Zircon zonation patterns as revealed by cathodoluminescence and backscattered electron images: Implications for interpretation of complex crustal histories. Chemical Geology 110:1– 13.

Harrison TM, Watson EB (1983) Kinetics of zircon dissolution and zirconium diffusion in granitic melts of variable water content. Contributions to Mineralogy and Petrology 84:66– 72.

Hawkesworth CJ, Kemp AIS (2006) Using hafnium and oxygen isotopes in zircons to unravel the record of crustal evolution. Chemical Geology 226:144– 162.

Hietpas J, Samson S, Moecher D, Chakraborty S (2011) Enhancing tectonic and provenance information from detrital zircon studies: assessing terrane-scale sampling and grain-scale characterization. Journal of the Geological Society of London 168:309–318.

Hoinkes G, Koller F, Demény A, Schuster R, Miller C, Thöni M, Kurz W, Krenn K, Walter F (2010) Metamorphism in the Eastern Alps. Acta Mineralogica-Petrographica, Field Guide Series 1:1–47.

Howard KE, Hand M, Barovich KM, Reid A, Wade BP, Belousova EA (2009) Detrital zircon ages: Improving interpretation via Nd and Hf isotopic data. Chemical Geology 262:277– 292.

Johnsson MJ (1993) The system controlling the composition of clastic sediments. In: Johnsson MJ, Basu A (eds) Processes Controlling the Composition of Clastic Sediments, Geological Society of America Special Paper 284, Boulder, pp 1– 20.

Kebede T, Klötzli U, Kosler J, Skiöld T (2005) Understanding pre-Variscan and Variscan basement components of the central Tauern Window, Eastern Alps (Austria): constraints from new single zircon U–Pb geochronology. International Journal of Earth Sciences 94:336–353.

Kemp AIS, Foster GL, Scherstén A, Whitehouse MJ, Darling J, Storey C (2009) Concurrent Pb–Hf isotope analysis of zircon by laser ablation multi-collector ICPMS, with implications for the crustal evolution of Greenland and the Himalayas. Chemical Geology 261:244–260.

Kinny PD, Maas R (2003) Lu-Hf and Sm-Nd isotope systems in zircon. In: Hanchar JM, Hoskin PWO (eds) Zircon, Reviews in Mineralogy and Geochemistry 53, pp 327– 341.

Klötzli US, Parrish RR (1996) Zircon U/Pb and Pb/Pb geochronology of the Rastenberg graniodiorite, South Bohemian Massif, Austria. Mineralogy and Petrology 58:197– 214.

Klötzli US, Frank W, Scharbert S, Thöni M (1999) The evolution of the SE Bohemian Massif based on geochronological data: a review. Jahrbuch der Geologischen Bundesanstalt 141:377–394.

Klötzli US, Koller F, Scharbert S, Höck V (2001) Cadomian lower-crustal contributions to Variscan granite petrogenesis (South Bohemian Pluton, Austria): constraints from zircon typology and geochronology, whole-rock, and feldspar Pb-Sr isotope systematics. Journal of Petrology 42:1621– 1642.

Klötzli U, Klötzli E, Günes Z, Košler J (2009) External accuracy of laser ablation U‒ Pb zircon dating: results from a test using five different reference zircons. Geostandards and Geoanalytical Research 33:5‒ 15.

Klötzli-Chowanetz E, Klötzli U, Koller F (1997) Lower Ordovician migmatisation in the Ötztal crystalline basement (Eastern Alps, Austria): linking U–Pb and Pb–Pb dating with zircon morphology. Schweizerische Mineralogische und Petrographische Mitteilungen 77:315–324.

Kröner A, Wendt I, Liew TC, Compston W, Todt W, Fiala J, Vankova V, Vanek J (1988) U-Pb zircon and Sm-Nd model ages of high-grade Moldanubian metasediments, Bohemian Massif, Czechoslovakia. Contributions to Mineralogy and Petrology 99:257‒ 266.

Košler J, Konopásek J, Sláma J, Vrána S (2014) U‒ Pb zircon provenance of Moldanubian metasediments in the Bohemian Massif. Journal of the Geological Society, London 171:83‒ 95.

Krogh TE (1982) Improved accuracy of U‒ Pb zircon dating by selection of more concordant fractions using a high gradient magnetic separation technique. Geochimica et Cosmochimica Acta 46:631‒ 635.

Linnemann U, Pereira F, Jeffries TE, Drost K, Gerdes A (2008) The Cadomian Orogeny and the opening of the Rheic Ocean: The diachrony of geotectonic processes constrained by LA‒ ICP‒ MS U‒ Pb zircon dating (Ossa-Morena and Saxo-Thuringian Zones, Iberian and Bohemian Massifs). Tectonophysics 461:21‒ 43.

Lisá L (2004) Exoscopy of Moravian eolian sediments. Bulletin of Geosciences 79:177‒ 182.

Lisá L, Uher P (2006) Provenance of Würmian loess and loess-like sediments of Moravia and Silesia (Czech Republic): a study of zircon typology and cathodoluminescence. Geologica Carpathica 57:397‒ 403.

Lisá L, Buriánek D, Uher P (2009) New approach to garnet redistribution during aeolian transport. Geological Quarterly 53:333– 340.

Lomax J, Fuchs M, Preusser F, Fiebig M (2014) Luminescence based loess chronostratigraphy of the Upper Palaeolithic site Krems-Wachtberg, Austria. Quaternary International 351:88– 97.

Ludwig KR (2008) User's manual for Isoplot 3.70: a geochronological toolkit for Microsoft® Excel. Berkeley Geochronology Center Special Publication No 4, USA, p 76.

Malusa MG, Carter A, Limoncelli M, Villa IM, Garzanti E (2013) Bias in detrital zircon geochronology and thermochronometry. Chemical Geology 359:90–107.

Meinhold, G., Morton, A.C., Fanning, C.M., Frei, D., Howard, J.P., Phillips, R.J., Strogen, D., Whitham, A.G., 2011. Evidence from detrital zircons for recycling of Mesoproterozoic and Neoproterozoic crust recorded in Paleozoic and Mesozoic sandstones of southern Libya. Earth and Planetary Science Letters 312:164–175.

Meinhold, G., Morton, A.C., Avigad, D., 2013. New insights into peri-Gondwana paleogeography and the Gondwana super-fan system from detrital zircon U–Pb ages. Gondwana Research, 23:661–665

Miller C, Konzett J, Tiepolo M, Armstrong RA, Thöni M (2007) Jadeite-gneiss from the Eclogite Zone, Tauern Window, Eastern Alps, Austria: Metamorphic, geochemical and zircon record of a sedimentary protolith. Lithos 93:68–88.

Moecher DP, Samson SD (2006) Differential zircon fertility of source terranes and natural bias in the detrital zircon record: Implications for sedimentary provenance analysis. Earth and Planetary Science Letters 247:252– 266.

Nehyba S, Roetzel R (2004) The Hollabrunn-Mistelbach formation (Upper Miocene, Pannonian) in the Alpine-Carpathian Foredeep and the Vienna basin in lower Austria –

An example of a Coarse-grained Fluvial System. Jahrbuch des Geologischen Bundesanstalt 144:191– 221.

Neubauer F, Klötzli U, Poscheschnik P (2001) Two stages of Cadomian magmatism in the Alps recorded in Late Ordovician sandstones of the Carnic Alps: results from zircon Pb/Pb evaporation dating. 21st IAS Meeting of Sedimentology, pp 126–127.

Neubauer F, Frisch W, Hansen BT (2002) Early Palaeozoic tectonothermal events in basement complexes of the eastern Graywacke Zone (Eastern Alps): evidence from U–Pb zircon data. International Journal of Earth Sciences 91:775–786.

Nemchin AA, Cawood PA (2005) Discordance of the U–Pb system in detrital zircons: implication for provenance studies of sedimentary rocks. Sedimentary Geology 182:143–162.

Patchett PJ, Kouvo O, Hedge CE, Tatsumoto M (1981) Evolution of continental crust and mantle heterogeneity: evidence from Hf isotopes. Contributions to Mineralogy and Petrology 78:279–297.

Petrakakis K (1997) Evolution of Moldanubian rocks in Austria: review and synthesis. Journal of Metamorphic Geology 15:203–222.

Preusser F, Fiebig M (2009) European Middle Pleistocene loess chronostratigraphy: some considerations based on evidence from the Wels site, Austria. Quaternary International 198:37– 45.

Pullen A, Kapp P, McCallister AT, Chang H, Gehrels GE, Garzione CN, Heermance RV, Ding L (2011) Qaidam Basin and northern Tibetan Plateau as dust sources for the Chinese Loess Plateau and paleoclimatic implications. Geology 39:1031–1034.

Pupin JP (1980) Zircon and granite petrology. Contributions to Mineralogy and Petrology 73:207–220.

Pye K (1995) The nature, origin and accumulation of loess. Quaternary Science Reviews 14:653‒ 667.

Reitner JM (2007) Glacial dynamics at the beginning of Termination I in the Eastern Alps and their stratigraphic implications. Quaternary International 164–165:64–84.

Renssen H, Kasse C, Vandenberghe J, Lorenz SJ (2007) Weichselian Late Pleniglacial surface winds over northwest and central Europe: a model‒ data comparison. Journal of Quaternary Science 22:281‒ 293.

Richter S, Goldberg SA, Mason PB, Traina AJ, Schwieters JB (2001) Linearity tests for secondary electron multipliers used in isotope ratio mass spectrometry. International Journal of Mass Spectrometry 206:105‒ 127.

Samson SD, D'Lemos RS, Miller BV, Hamilton MA (2005) Neoproterozoic palaeogeography of the Cadomia and Avalon terranes: constraints from detrital zircon U–Pb ages. Journal of the Geological Society, London 162:65‒ 71.

Scherer EE, Whitehouse MJ, Münker C (2007) Zircon as a monitor of crustal growth. In: Harley SL, Kelly NM (eds) Zircon: Tiny but Timely, Elements 3, pp 19‒ 24.

Schmid SM, Fügenschuh B, Kissling E, Schuster R (2004) Tectonic map and overall architecture of the Alpine orogen. Eclogae Geologicae Helvetiae 97:93–117.

Shao Y (2009) Physics and Modelling of Wind Erosion. In: Atmospheric and Oceanographic Sciences Library, vol. 37. Springer, Netherlands, ISBN 978-1-4020-8894-0. http://dx.doi.org/10.1007/978-1-4020-8895-7.

Siebel W, Chen F (2010) Zircon Hf isotope perspective on the origin of granitic rocks from eastern Bavaria, SW Bohemian Massif. International Journal of Earth Sciences 99:993–1005.

Siebel W, Thiel M, Chen F (2006) Zircon geochronology and compositional record of late- to post-kinematic granitoids associated with the Bavarian Pfahl zone (Bavarian Forest). Mineralogy and Petrology 86:45–62.

Siebel W, Shang CK, Reitter E, Rohrmüller J, Breiter K (2008) Two distinctive granite suites in the south-western Bohemian Massif and their record of emplacement: constraints from zircon $^{207}Pb/^{206}Pb$ chronology and geochemistry. Journal of Petrology 49:1853–1872.

Siebel W, Shang CK, Thern E, Danišík M, Rohrmüller J (2012) Zircon response to high-grade metamorphism as revealed by U–Pb and cathodoluminescence studies. International Journal of Earth Sciences 101:2105–2123.

Siegesmund S, Heinrichs T, Romer RL, Doman D (2007) Age constraints on the evolution of the Austroalpine basement to the south of the Tauern Window. International Journal of Earth Sciences 96:415–432.

Sláma J, Košler J (2012) Effects of sampling and mineral separation on accuracy of detrital zircon studies. Geochemistry, Geophysics, Geosystems 13:Q05007, doi: 10.1029/2012GC004106.

Sláma J, Košler J, Condon DJ, Crowley JL, Gerdes A, Hanchar JM, Horstwood MSA, Morris GA, Nasdala L, Norberg N, Schaltegger U, Schoene B, Tubrett MN, Whitehouse MJ (2008) Plešovice zircon — A new natural reference material for U – Pb and Hf isotopic microanalysis. Chemical Geology 249:1–35.

Smalley I, O'Hara-Dhand K, Wint J, Machalett B, Jary Z, Jefferson I (2009) Rivers and loess: the significance of long river transportation in the complex event-sequence approach to loess deposit formation. Quaternary International 198:7–18.

Söderlund U, Patchett JP, Vervoort JD, Isachsen C (2004) The ^{176}Lu decay constant determined by Lu–Hf and U–Pb isotope systematics of Precambrian mafic intrusions. Earth and Planetary Science Letters 219:311–324.

Stampfli GM, von Raumer JF, Borel GD (2002) Paleozoic evolution of pre-Variscan terranes: From Gondwana to the Variscan collision. In: Martínez Catalán JR, Hatcher RD Jr, Arenas R, Díaz García F (eds) Variscan-Appalachian dynamics: The building of the late Paleozoic basement, Geological Society of America Special Paper 364, pp 263–280.

Stevens T, Palk C, Carter A, Lu H, Clift PD (2010) Assessing the provenance of loess and desert sediments in northern China using U–Pb dating and morphology of detrital zircons. Geological Society of America Bulletin 122:1331–1344.

Stevens T, Carter A, Watson TP, Vermeesch P, Andó S, Bird AF, Lu H, Garzanti E, Cottam MA, Sevastjanova I (2013) Genetic linkage between the Yellow River, the Mu Us desert and the Chinese Loess Plateau. Quaternary Science Reviews 78:355– 368.

Sylvester PJ, Ghaderi M (1997) Trace element analysis of scheelite by excimer laser ablation inductively coupled plasma mass spectrometry (ELA-ICP-MS) using a synthetic silicate glass standard. Chemical Geology 141:49– 65.

Tait JA, Bachtadse V, Franke W, Soffel HC (1997) Geodynamic evolution of the European Variscan fold belt: palaeomagnetic and geological constraints. Geologische Rundschau 86:585– 598.

Teipel U,·Eichhorn R,·Loth G, Rohrmüller J, Höll R, Kennedy A (2004) U-Pb SHRIMP and Nd isotopic data from the western Bohemian Massif (Bayerischer Wald, Germany): Implications for Upper Vendian and Lower Ordovician magmatism. International Journal of Earth Sciences 93:782– 801.

Terhorst B, Ottner F, Wriessnig K (2012) Weathering intensity and pedostratigraphy of the Middle to Upper Pleistocene loess/palaeosol sequence of Wels-Aschet (Upper Austria). Quaternary International 265:142–154.

Thiel C, Buylaert J-P, Murray A, Terhorst B, Hofer I, Tsukamoto S, Frechen M (2010) Luminescence dating of the Stratzing loess profile (Austria) – testing the potential of an elevated temperature post-IR IRSL protocol. Quaternary International 234:23–31.

Tsoar H, Pye K (1987) Dust transport and the question of desert loess formation. Sedimentology 34:139–153.

Újvári G, Varga A, Balogh-Brunstad Z (2008) Origin, weathering, and geochemical composition of loess in southwestern Hungary. Quaternary Research 69:421–437.

Újvári G, Varga A, Ramos FC, Kovács J, Németh T, Stevens T (2012) Evaluating the use of clay mineralogy, Sr–Nd isotopes and zircon U–Pb ages in tracking dust provenance: an example from loess of the Carpathian Basin. Chemical Geology 304–305:83–96.

Újvári G, Klötzli U, Kiraly F, Ntaflos T (2013) Towards identifying the origin of metamorphic components in Austrian loess: insights from detrital rutile chemistry, thermometry and U–Pb geochronology. Quaternary Science Reviews 75, 132–142.

van Husen D (1981) Geologisch-sedimentologische Aspekte im Quartär von Österreich. Mitteilungen der Geologischen Gesellschaft 74/75:197–230.

van Husen D (2000) Geological processes during the Quaternary. Mitteilungen der Geologischen Gesellschaft 92:135–156.

Veselá P, Söllner F, Finger F, Gerdes A (2011) Magmato-sedimentary Carboniferous to Jurassic evolution of the western Tauern window, Eastern Alps (constraints from U-Pb zircon dating and geochemistry). International Journal of Earth Sciences 100:993–1027.

Vermeesch P (2004) How many grains are needed for a provenance study? Earth and Planetary Science Letters 224:441–451.

Vermeesch P (2012) On the visualisation of detrital age distributions. Chemical Geology 312– 313:190– 194.

Vervoort JD, Patchett PJ, Albarède F, Blichert-Toft J, Rudnick R, Downes H (2000) Hf–Nd isotopic evolution of the lower crust. Earth and Planetary Science Letters 181:115–129.

Vervoort JD, Patchett PJ, Söderlund U, Baker M (2004) Isotopic composition of Yb and the determination of Lu concentrations and Lu/Hf by isotope dilution using MC-ICPMS. Geochemistry, Geophysics, Geosystems 5, Q11002, doi:10.1029/2004GC000721.

von Quadt A (1992) U-Pb zircon and Sm-Nd isotope geochronology of mafic and ultramafic rocks from the central part of the Tauern Window (eastern Alps). Contributions to Mineralogy and Petrology 110:57– 67.

Watson EB (1996) Dissolution, growth and survival of zircons during crustal fusion: Kinetic principles, geological models and implications for isotopic inheritance. Transactions of the Royal Society of Edinburgh: Earth Sciences 87:43– 56.

Watson EB, Harrison TM (1983) Zircon saturation revisited: temperature and composition effects in a variety of crustal magma types. Earth and Planetary Science Letters 64:295– 304.

Weber B, Scherer EE, Martens UK, Mezger K (2012) Where did the lower Paleozoic rocks of Yucatan come from? A U–Pb, Lu–Hf, and Sm–Nd isotope study. Chemical Geology 312– 313:1– 17.

Wendt JI, Kröner A, Fiala J, Todt W (1994) U–Pb zircon and Sm–Nd dating of Moldanubian HP/HT granulites from South Bohemia, Czech Republic. Journal of the Geological Society 151:83–90.

Whitehouse MJ, Kamber BS, Moorbath S (1999) Age significance of U–Th–Pb zircon data from early Archaean rocks of west Greenland—a reassessment based on combined ion-microprobe and imaging studies. Chemical Geology 160:201– 224.

Woodhead JD, Hergt JM (2005) A preliminary appraisal of seven natural zircon reference materials for in situ Hf isotope determination. Geostandards and Geoanalytical Research 29:183–195.

Xiao G, Zong K,, Li G, Hu Z, Dupont-Nivet G, Peng S, Zhang K (2012) Spatial and glacial-interglacial variations in provenance of the Chinese Loess Plateau. Geophysical Research Letters 39:L20715, doi:10.1029/2012GL053304.

Figure captions

Fig. 1 Simplified geological map of the northeastern part of Austria (modified after Beck–Mannagetta 1964; Haase et al. 2007) with the sampling sites. The numbers mark the sampling localities: 1. Krems (sample K23), 2. Stratzing (sample S1), 3. Wels (sample A16). Letters denote geological units, formations, etc. mentioned in chapter ‘Geological setting’: A. Gföhl unit, B. Varied series, C. Monotonous series, D. South Bohemian Pluton, E. Hollabrunn-Mistelbach Formation, F. Rhenodanubian flysch zone, G. Austroalpine unit, H. Tauern window (Penninic)

Fig. 2 Secondary electron and cathodoluminescence images of detrital zircons from samples K23 (a, b) and A16 (c, d), with U– Pb ages. Panels a), c) and d) show typical igneous zircons with magmatic growth zoning. Resorption and reprecipitation/recrystallization features are visible in zircon shown in panel a), while panel b) displays a metamorphic zircon with recrystallization rims. The abbreviation ‘conc.’ means concordance. Ages younger than 1.0 Ga are $^{206}Pb/^{238}U$ ages, while those older than 1.0 Ga are $^{207}Pb/^{206}Pb$ ages. White lines denote the axis of laser ablation trenches. Their diameters are given after the @ in microns

Fig. 3 Secondary electron and cathodoluminescence images of detrital zircons from sample S1 with U– Pb ages and Hf isotopic compositions. Magmatic zircons with oscillatory zoning (panels a, c, e, f), metamorphic zircon (panel b), and a zircon with inherited/xenocrystic core (panel d). The abbreviation ‘conc.’ means concordance. Ages younger than 1.0 Ga are $^{206}Pb/^{238}U$ ages, while those older than 1.0 Ga are $^{207}Pb/^{206}Pb$ ages. White lines denote the axis of laser ablation trenches. Their diameters are given after the @ in microns

Fig. 4 Kernel density estimates of zircon U– Pb ages of the three studied loess samples. Black lines are distributions estimated from U– Pb ages with age uncertainties <20% and cutoff at 20% (e_20, c_20), while gray/turquoise shaded distributions are calculated from U– Pb ages having <10% uncertainties and cutoff at 10% (e_10, c_10). Number of ages (n) used in these calculations are also specified. All the KDEs have been calculated using a bandwidth of 25 Ma. Bold numbers are age components calculated by mixture modeling in DensityPlotter. Panels (right up corner) are blow ups of the distributions for a period of 200 to 800 Ma. White/red dots mark purely magmatic ages (based on CL images), while gray filled dots denote metamorphic ages. Abbreviations: Var. = Variscan (320-360 Ma), Cal. = Caledonian (420-480 Ma) and Cad./P.A. = Cadomian/Pan-African (500-800 Ma)

Fig. 5 Age versus a) $^{176}Hf/^{177}Hf_t$ and b) $\varepsilon\ Hf_t$ diagrams for detrital zircon grains from loess samples S1, K23 and A16. Zircons listed in Table 2 are plotted exclusively. Dashed lines illustrate typical evolution paths of crust separated from a depleted mantle at different times in Ma (crustal residence ages) with $^{176}Lu/^{177}Hf$ of 0.015 (Condie et al. 2005)

Figure1_col
Click here to download high resolution image

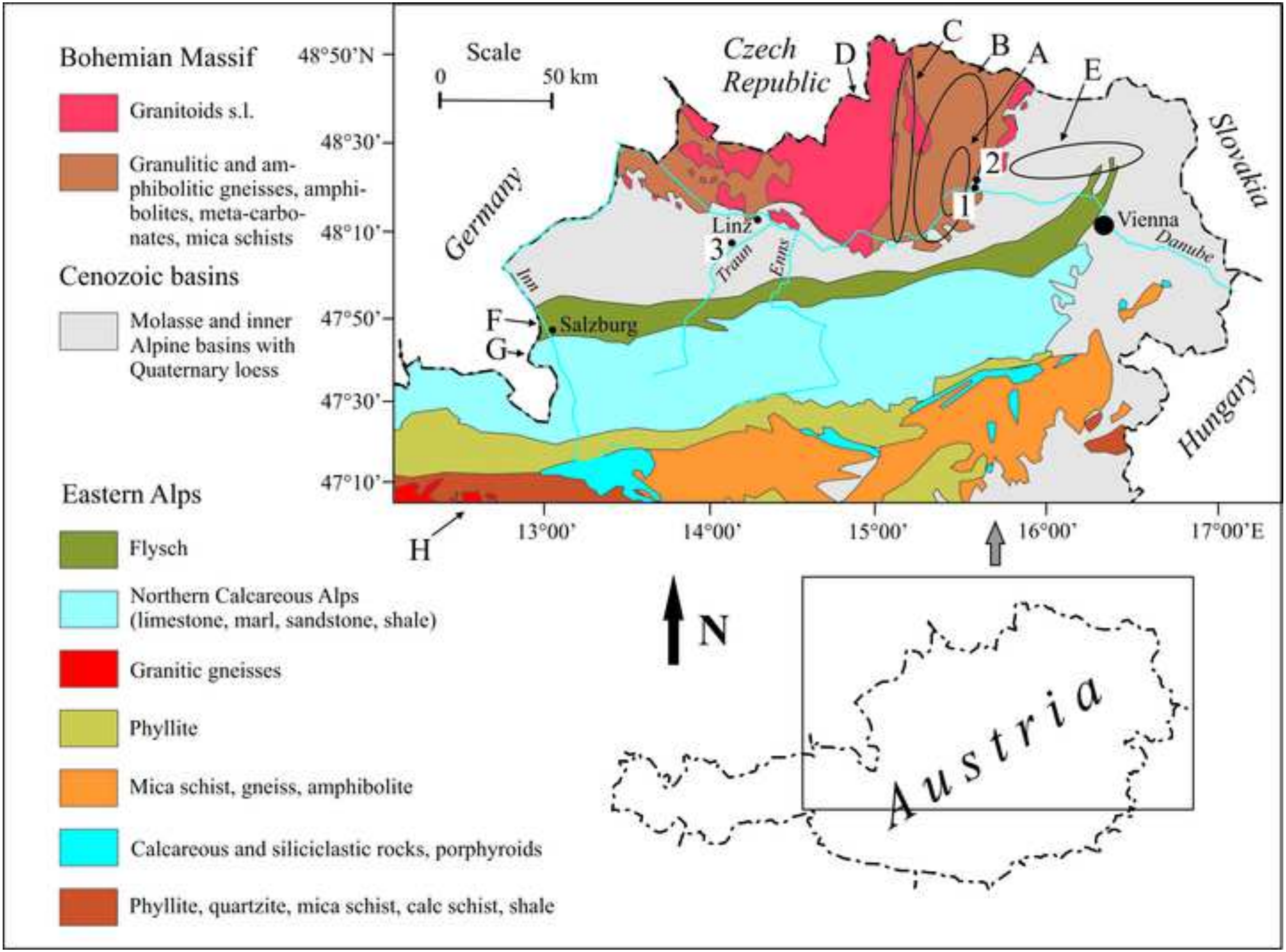

Figure1_bw
Click here to download high resolution image

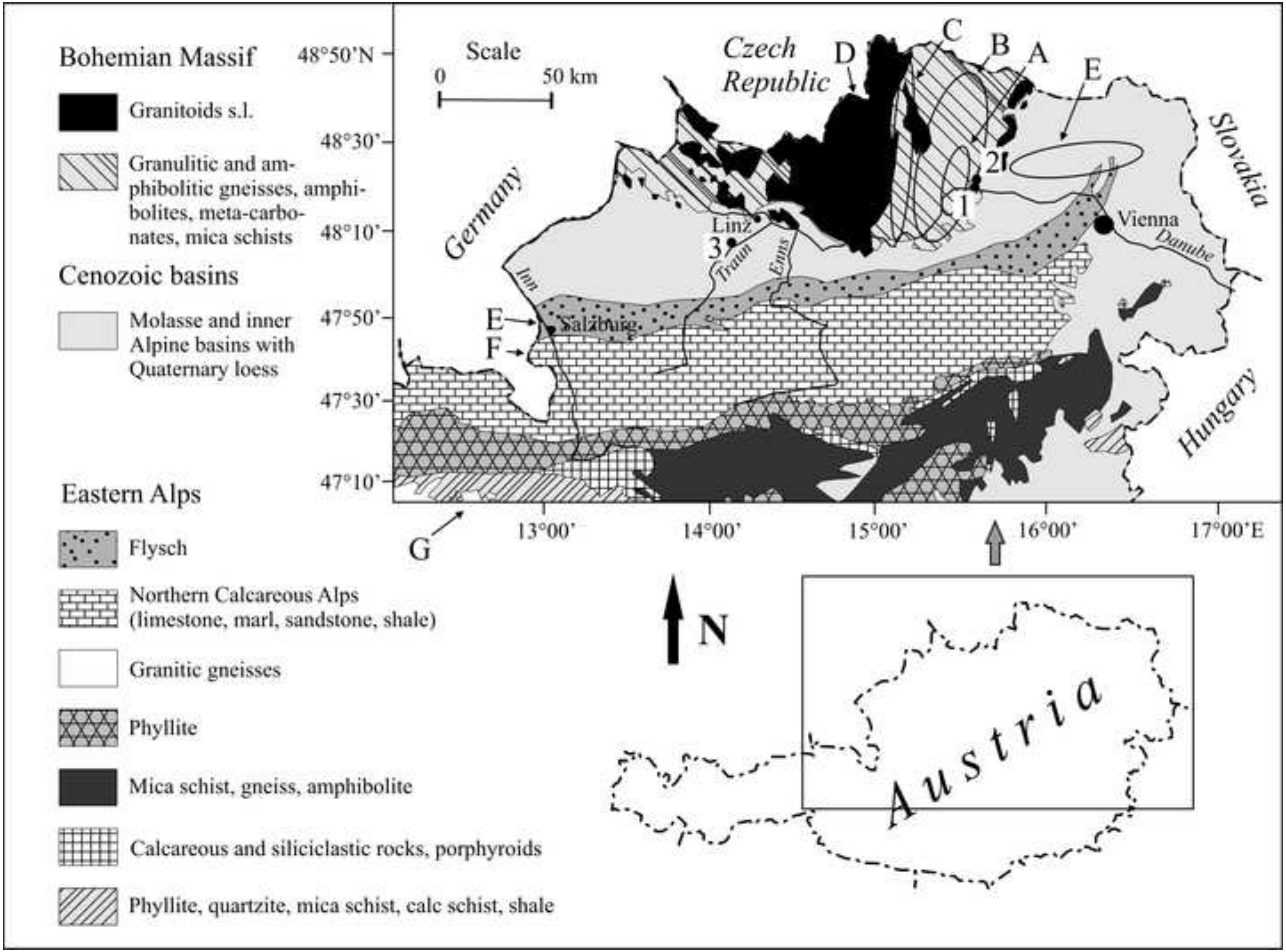

Figure2_bw

Click here to download high resolution image

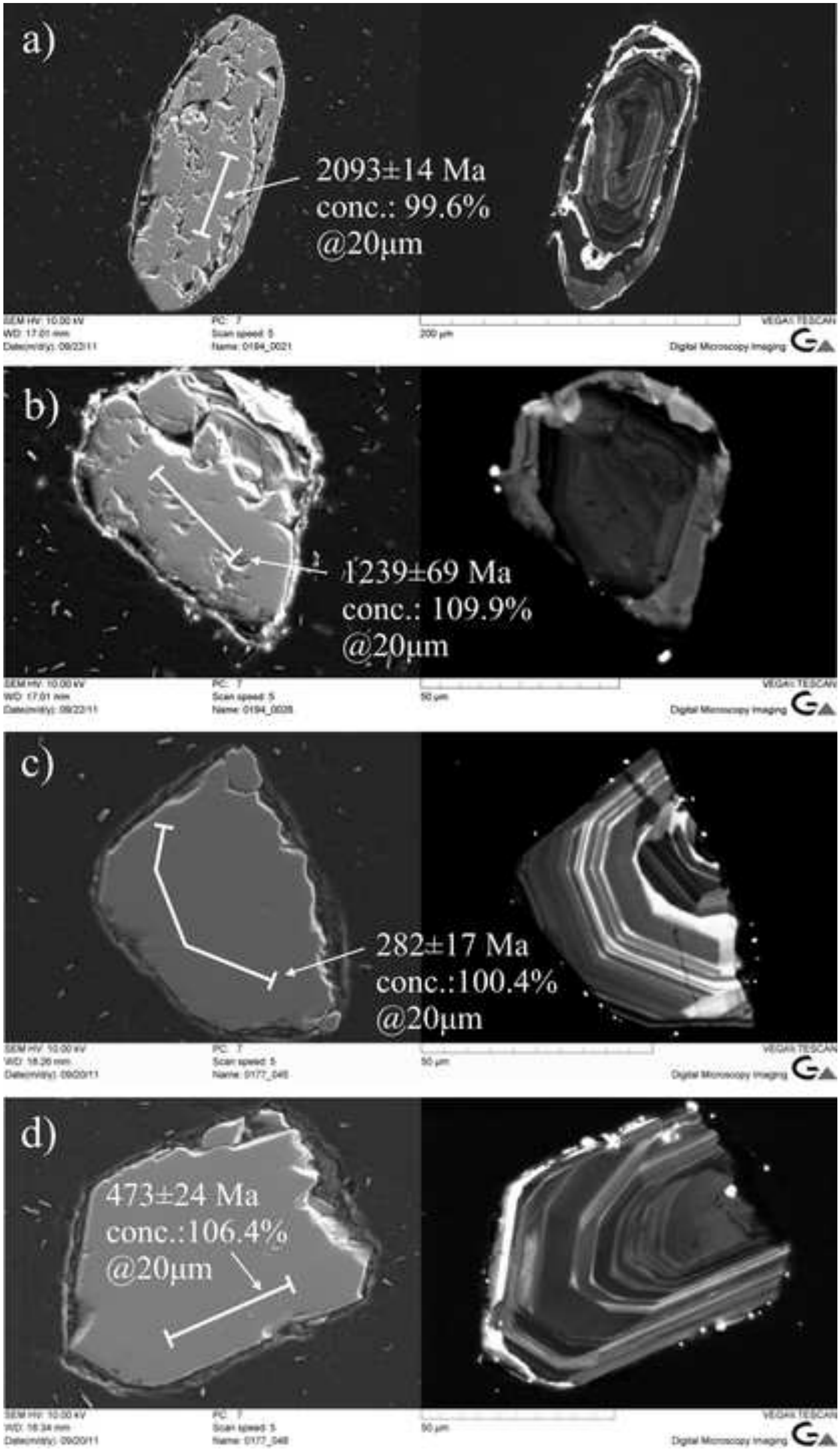

Figure3_bw
Click here to download high resolution image

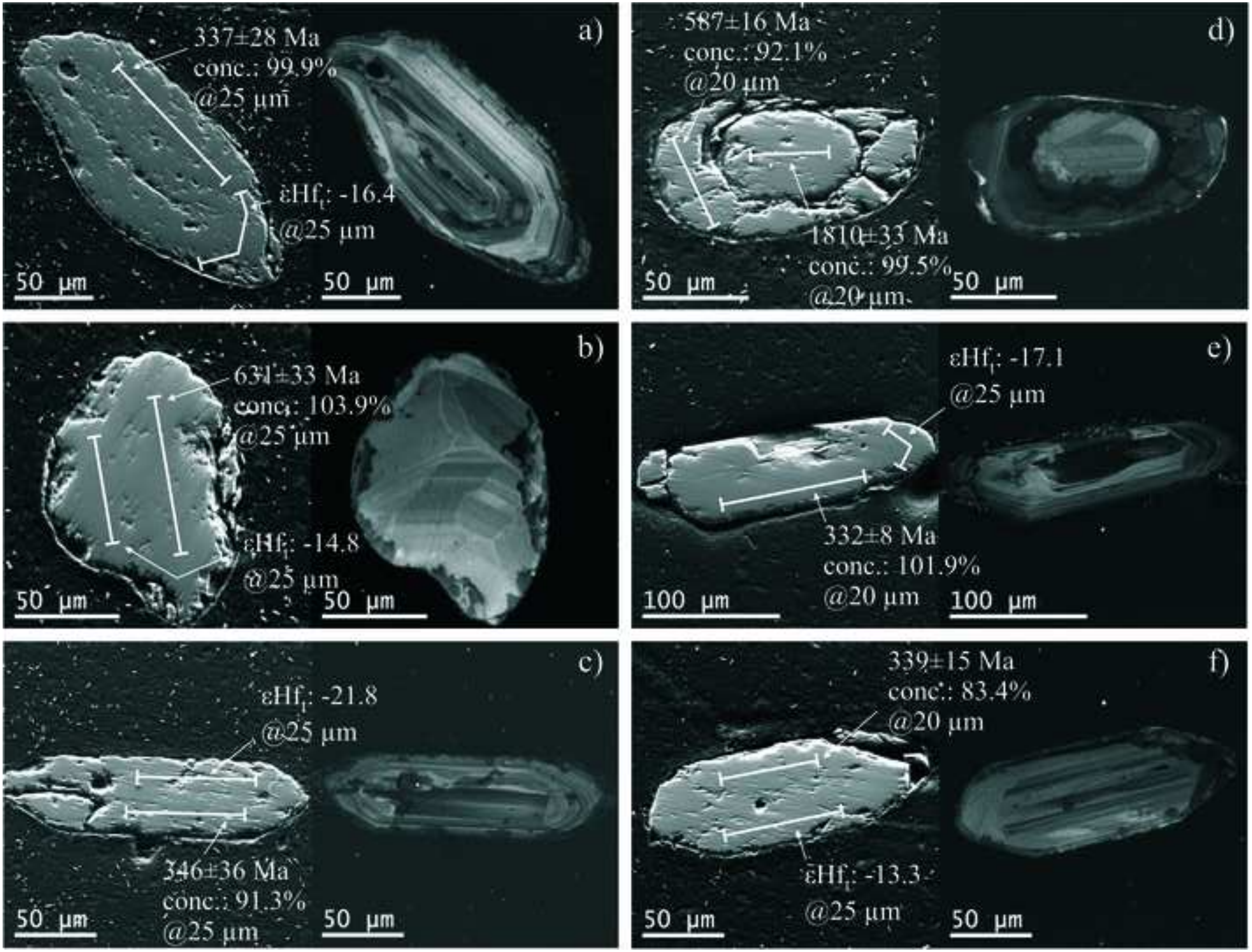

Figure4_col

Click here to download high resolution image

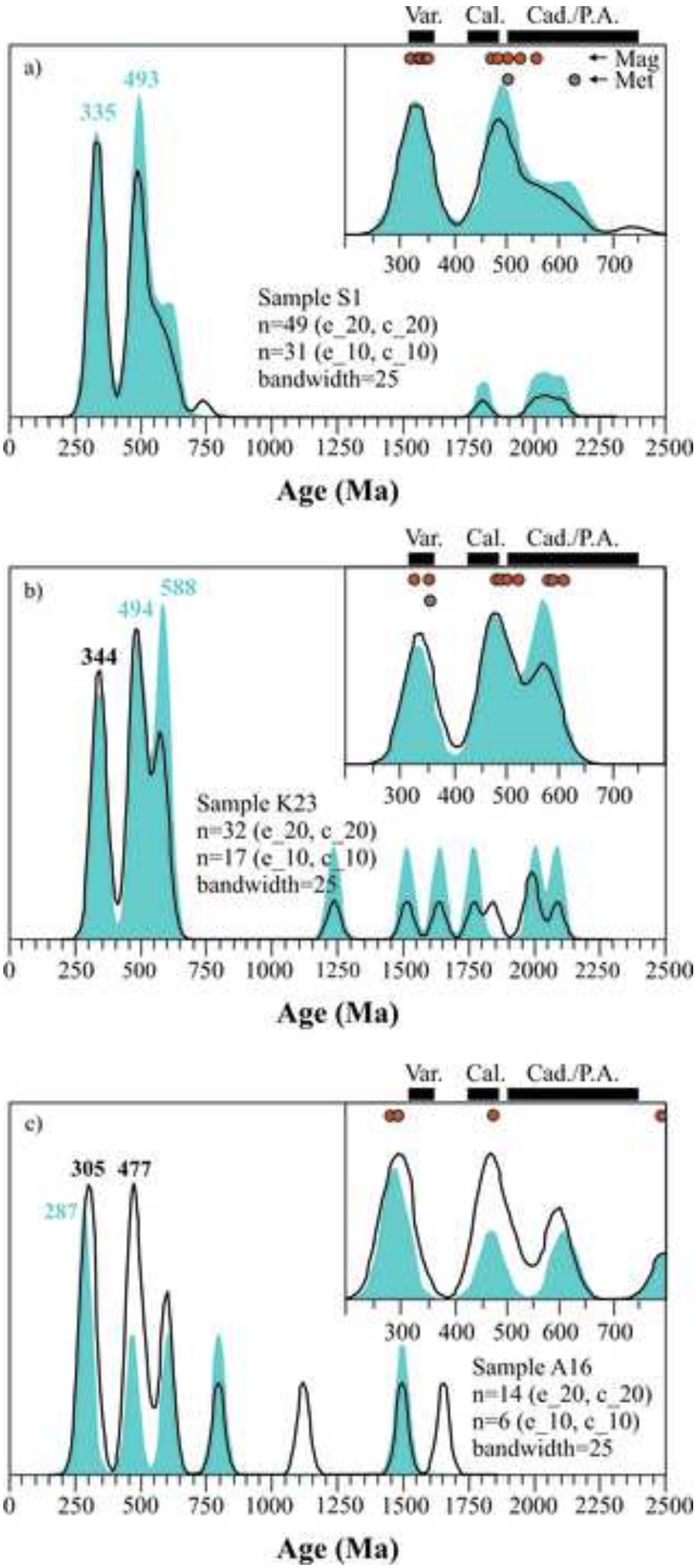

Figure4_bw

Click here to download high resolution image

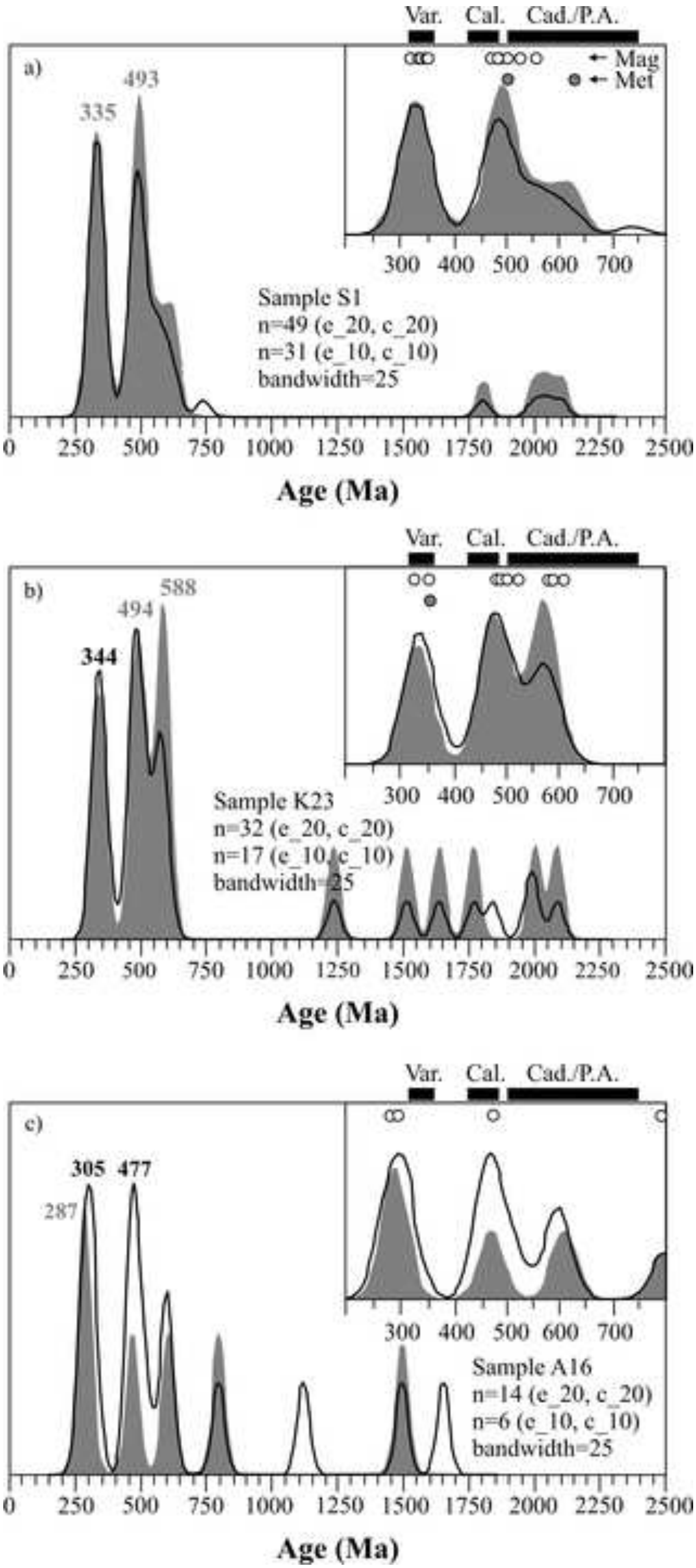

Figure5_col

Click here to download high resolution image

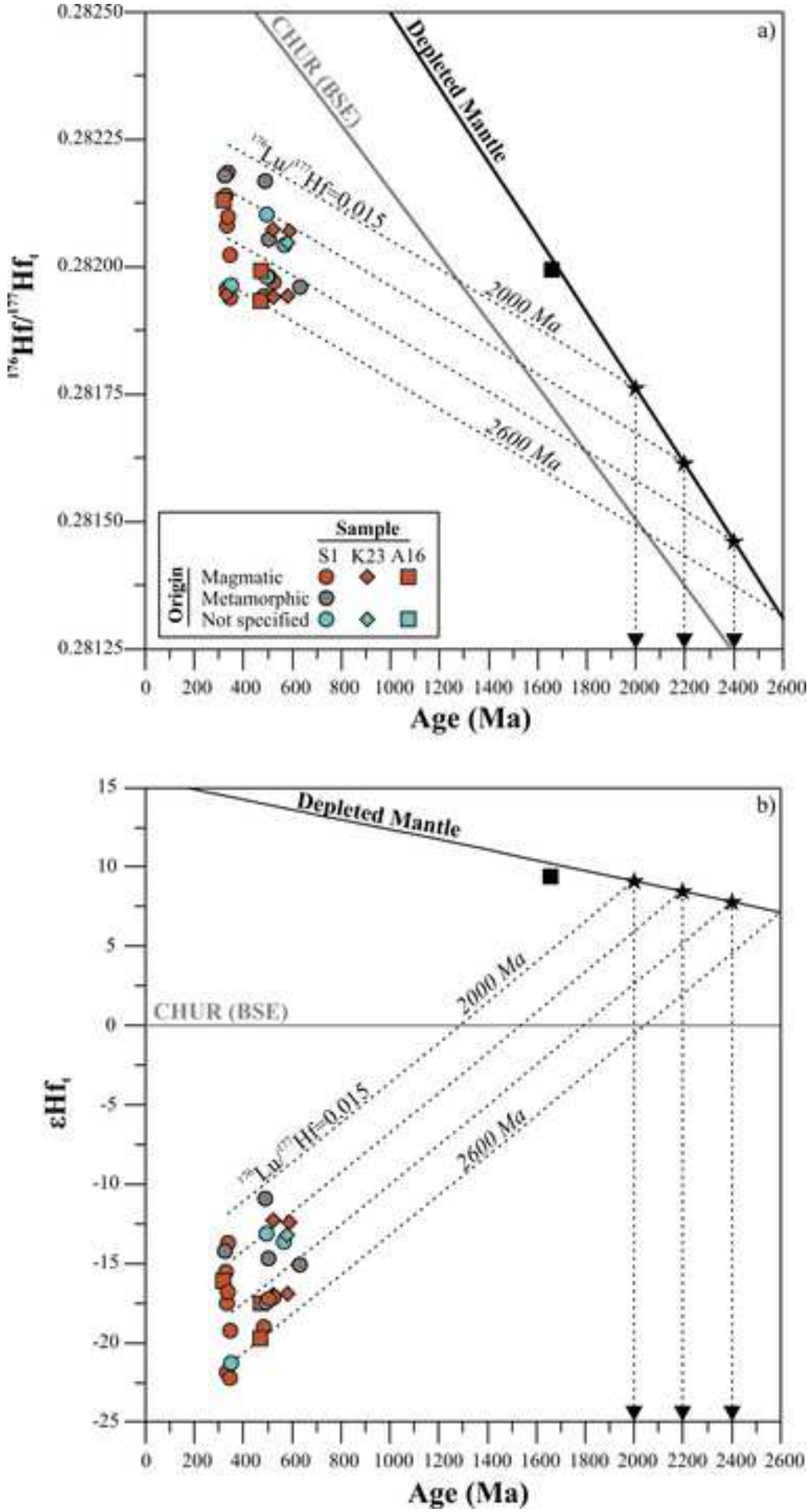

Figure5_bw

Click here to download high resolution image

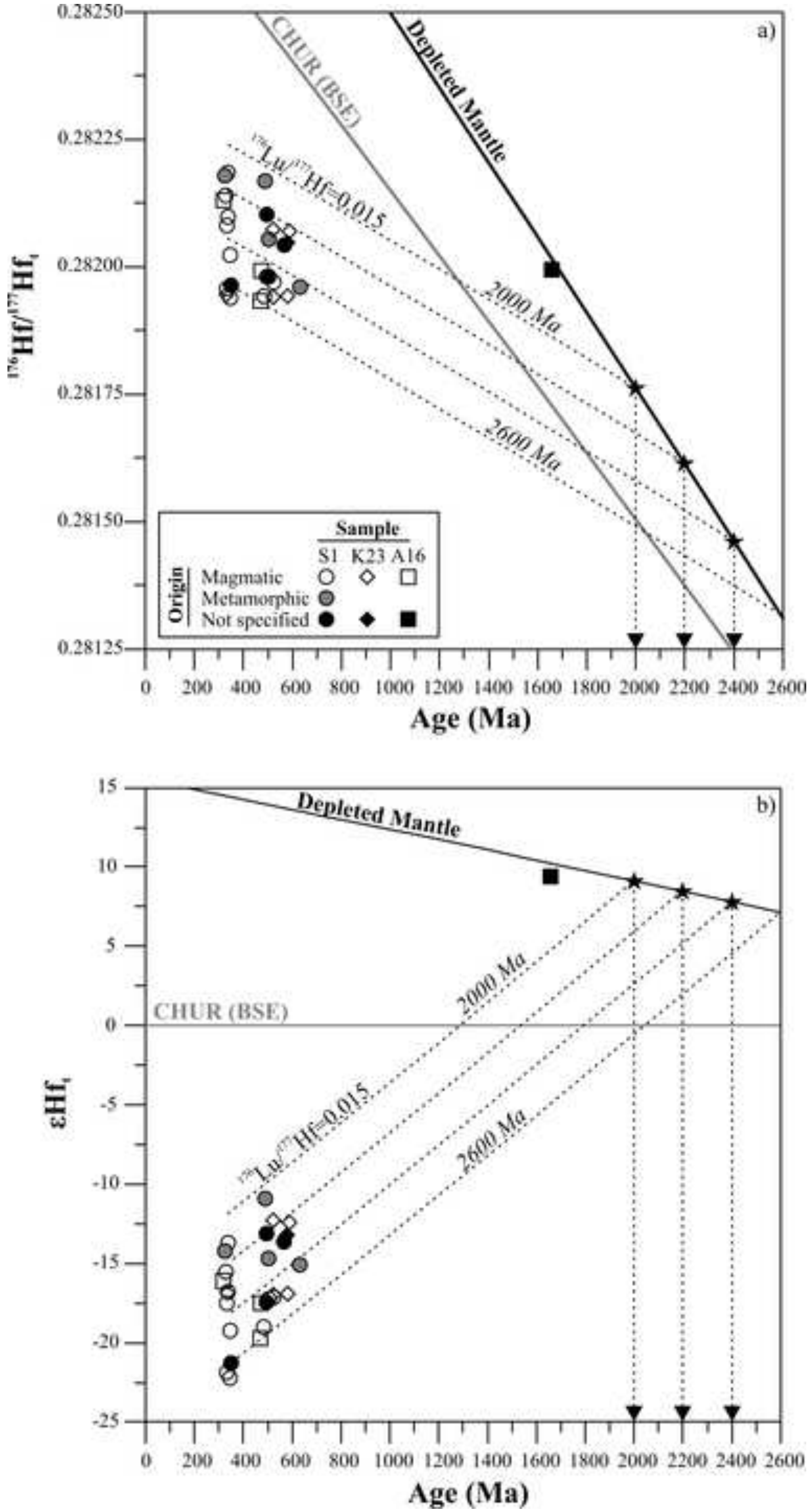

Table 1. Likelihoods of missing age populations for the analyzed loess samples based on binomial probability (after Andersen 2005)

Sample	Number of zircons	Concordance criteria	Detection limit at p_L=0.5[a]	Detection limit at p_L=0.95[b]	Failure rate (%) at X_i=10%[c]	Failure rate (%) at X_i=20%	Failure rate (%) at X_i=40%
S1	49	<20%	1.4	5.9	0.6	0.0	0.0
	31	<10%	2.2	9.2	3.8	0.1	0.0
K23	32	<20%	2.1	8.9	3.4	0.1	0.0
	17	<10%	4.0	16.2	16.7	2.3	0.0
A16	14	<20%	4.8	19.3	22.9	4.4	0.1
	6	<10%	10.9	39.3	53.1	26.2	4.7

[a]Detection limit is the percent abundance of the largest population of zircons likely to remain undetected in *n* analyses, for a probability level (p_L) of 0.5. It is calculated as $X_L = \ 1- \ 1-p_L{}^{\frac{1}{n}} \times 100$ (Andersen 2005). Detection limit at p_L=0.5 marks an upper abundance limit for populations that are more probably overlooked than observed in *n* analyses

[b]Detection limit is the percent abundance of the largest population of zircons likely to remain undetected in *n* analyses, for a probability level (p_L) of 0.95

[c]Failure rate (in percent) is the probability of overlooking an age population with an abundance X_i in the sediment, and calculated as $p_{n_i=0} = ((1-X_i)^n) \times 100$ (Andersen 2005)

Table2

Table 2. U– Pb ages and Lu– Hf isotopic compositions of detrital zircons from loess samples S1, K23, and A16

Sample code	$^{206}Pb/^{238}U$ age (Ma)	±2σ (Ma)	Conc. (%)[a]	$^{176}Hf/^{177}Hf$	±2SE	$^{176}Lu/^{177}Hf$	±2SE	εHf_0[b]	±2σ[c]	$^{176}Hf/^{177}Hf_t$[d]	±2σ[e]	εHf_t[f]	τ^c_{DM}-Hf (Ma)[g]	Origin
sample S1														
120316_0155_S1_003a,d	349	12	86.8	0.281965	0.000456	0.000145	0.000007	-29.0	0.2	0.281964	0.000456	-21.3	2600	not specified
120316_0155_S1_022a,d	495	29	109.1	0.282125	0.000389	0.002378	0.000022	-23.4	0.1	0.282102	0.000389	-13.1	2206	not specified
120316_0155_S1_023a,d	503	38	105.0	0.282065	0.000459	0.001141	0.000023	-25.5	0.2	0.282054	0.000459	-14.7	2308	metamorphic
120316_0155_S1_025a,d	337	28	99.9	0.282105	0.000566	0.001005	0.000023	-24.1	0.2	0.282098	0.000566	-16.8	2313	magmatic
120317_0155_S1_032a,d	485	11	100.6	0.281965	0.000444	0.002479	0.000042	-29.0	0.2	0.281943	0.000444	-19.0	2563	magmatic
120317_0155_S1_040a,d	328	11	114.9	0.282145	0.000656	0.000846	0.000057	-22.6	0.2	0.282140	0.000656	-15.5	2228	magmatic
120317_0155_S1_047a,d	631	33	103.9	0.281963	0.000455	0.000194	0.000006	-29.1	0.2	0.281960	0.000455	-15.1	2433	metamorphic
120317_0155_S1_054a,d	325	35	88.0	0.282186	0.000526	0.001101	0.000022	-21.2	0.2	0.282179	0.000526	-14.2	2143	metamorphic
120317_0155_S1_059a,d	346	36	91.3	0.281946	0.000560	0.000969	0.000010	-29.7	0.2	0.281940	0.000560	-22.2	2655	magmatic
120317_0155_S1_064a,d	523	17	99.0	0.281989	0.000715	0.001828	0.000036	-28.2	0.3	0.281971	0.000715	-17.1	2478	magmatic
120317_0155_S1_065a,d	503	27	98.5	0.282005	0.000606	0.002595	0.000073	-27.6	0.2	0.281981	0.000606	-17.2	2468	magmatic
120317_0155_S1_078a,d	333	29	110.8	0.281965	0.000733	0.001088	0.000035	-29.0	0.3	0.281958	0.000733	-21.9	2623	magmatic
120317_0155_S1_089a,d	332	8	101.9	0.282087	0.000541	0.000946	0.000016	-24.7	0.2	0.282082	0.000541	-17.5	2353	magmatic
120317_0155_S1_094a,d	566	18	98.4	0.282050	0.000478	0.000684	0.000025	-26.0	0.2	0.282043	0.000478	-13.6	2292	not specified
120317_0155_S1_096a,d	489	55	107.2	0.282181	0.000718	0.001366	0.000038	-21.4	0.3	0.282169	0.000718	-10.9	2064	metamorphic
120319_0155_S1_097a,d	494	19	85.4	0.281990	0.000562	0.001023	0.000007	-28.1	0.2	0.281981	0.000562	-17.4	2473	not specified
120319_0155_S1_099b,d	339	15	83.4	0.282191	0.000568	0.000850	0.000040	-21.0	0.2	0.282185	0.000568	-13.7	2121	magmatic
120319_0155_S1_103a,d	346	27	114.4	0.282031	0.000497	0.001159	0.000012	-26.7	0.2	0.282023	0.000497	-19.2	2472	magmatic
sample K23														
120320_0194_K23_022a,d	579	16	101.3	0.282056	0.000769	0.000807	0.000026	-25.8	0.3	0.282047	0.000769	-13.2	2276	not specified
120320_0194_K23_035a,d	522	14	88.6	0.281956	0.000754	0.001530	0.000044	-29.3	0.3	0.281941	0.000754	-17	2544	magmatic
120320_0194_K23_036a,d	522	12	109.1	0.282087	0.000764	0.001333	0.000024	-24.7	0.3	0.282074	0.000764	-12.3	2253	magmatic
120320_0194_K23_053a,d	332	55	107.1	0.281951	0.000669	0.000830	0.000019	-29.5	0.2	0.281945	0.000669	-16.8	2651	magmatic
120320_0194_K23_054a,d	589	56	108.9	0.282084	0.000783	0.001260	0.000038	-24.8	0.3	0.282070	0.000783	-12.4	2219	magmatic
120320_0194_K23_058a,d	581	35	118.2	0.281949	0.001002	0.000560	0.000039	-29.6	0.4	0.281943	0.001002	-16.9	2504	magmatic
sample A16														

120316_0176_A16_006a,d	319	23	82.4	0.282134	0.000967	0.000771	0.000018	-23.0	0.3	0.282130	0.000967	-16.1	2255	magmatic
120320_0177_A16_046a,d	1657*	102	87.7	0.282017	0.001518	0.000727	0.000019	-27.2	0.5	0.281994	0.001518	9.4	1712	not specified
120320_0177_A16_048a,d	473	24	106.4	0.282008	0.001020	0.001781	0.000018	-27.5	0.4	0.281992	0.001020	-17.5	2461	magmatic
120320_0177_A16_061a,d	469	38	118.3	0.281944	0.001819	0.001237	0.000028	-29.8	0.6	0.281933	0.001819	-19.7	2594	magmatic

Sample code: a/b denotes the U− Pb ages (see also the Supplementary Tables), d marks Lu− Hf analyses spots

[a]'Conc.' means concordance (206Pb/238U/207Pb/206Pb*100)

[b]ε Hf_0=($^{176}Hf/^{177}Hf_{zircon\text{-}meas.}/^{176}Hf/^{177}Hf_{CHUR\text{-}0}$− 1)*10000, where $^{176}Hf/^{177}Hf_{CHUR\text{-}0}$=0.282785±0.000011 (Bouvier et al. 2008)

[c]Uncertainties have been propagated as the root of the sum of the squared errors

[d]$^{176}Hf/^{177}Hf_t={}^{176}Hf/^{177}Hf_{zirc.} - {}^{176}Lu/^{177}Hf_{zirc.}(e^{\lambda t} - 1)$, where $\lambda=\lambda_{176Lu}=1.867\pm0.008\times10^{-11}$ a^{-1} (Söderlund et al. 2004), and *t* is the crystallization ages of zircons

[e]Uncertainties (σ) of $^{176}Hf/^{177}Hf_t$ have been propagated as

$\sigma_{176Hf/177Hf_t} = \sqrt{\sigma^2_{176Hf/177Hf_{zirc.}} + ((e^{\lambda t}-1)\sigma_{176Lu/177Hf_{zirc.}})^2 + ((e^{\lambda t}-1)176Lu/177Hf_{zirc.}t\sigma_\lambda)^2 + ((e^{\lambda t}-1)176Lu/177Hf_{zirc.}\lambda\sigma_t)^2}$. For the details of mathematical derivation of this expression see the Appendix

[f]ε Hf_t=[($^{176}Hf/^{177}Hf_{zirc.} - {}^{176}Lu/^{177}Hf_{zirc.}(e^{\lambda t} - 1)/ {}^{176}Hf/^{177}Hf_{CHUR\text{-}0} - {}^{176}Lu/^{177}Hf_{CHUR\text{-}0}(e^{\lambda t} - 1)$) − 1]*10000, where $^{176}Lu/^{177}Hf_{CHUR\text{-}0}$=0.0336±0.0001 (Bouvier et al. 2008)

[g]Two-stage crustal residence model ages were calculated as $\tau_{DM} - Hf = (1/\lambda)\ln(1+m)\,, where\ m = [176Hf/177Hf_{DM} - (176Hf/177Hf_{t,zirc.} + 176Lu/177Hf_{avg.crust}(e^{\lambda t} - 1))]/[176Lu/177Hf_{DM} - 176Lu/177Hf_{avg.crust}]$. We assumed $^{176}Lu/^{177}Hf_{avg.crust}$=0.015 (Griffin et al. 2004; Condie et al. 2005) and the present day depleted mantle (DM) model is based on $^{176}Hf/^{177}Hf_{DM}$=0.283224 (Vervoort et al. 2000), $^{176}Lu/^{177}Hf_{DM}$=0.03836 (calculated for εHf=0 at 4500 Ma, Weber et al. 2012)

*It is a $^{207}Pb/^{206}Pb$ age

Table3

Table 3. U-Pb ages of zircons from potential sources

Potential sources	Rock type	Ages (Ma)	Ages of inherited zircon cores (Ma)	Interpretation	$^{176}Hf/^{177}Hf_t$		ε Hf_t		References
					Max.	Min.	Max.	Min.	
Bohemian Massif, Moldanubian Zone									
Southwest part									
Sarleinsbach, S Bohemian Pluton, Austria	Weinsberg type granites	355±9 and 345±5	523±5	high-T metamorphism and Carboniferous partial melting					Klötzli et al. (2001)
Bavarian forest	metarhyolite, metabasite, metagranitoids	555±12 to 549±6, 486±7 to 480±6, 431±7, 319±5 to 316±10	2700 to 2000	Late Vendian and Early Ordovician magmatism and anatexis, Post-Cadomian and Variscan metamorphism					Teipel et al. (2004)
Pfahl zone, Bavarian forest	granite, granodiorite	329-321		Visean-Bashkirian magma emplacement					Siebel et al. (2006)
Bavarian and Ostrong terrane (Bavarian forest)	granite	328-321		granite formation during a short period of crustal melting					Siebel et al. (2008)
Palatinate and Bavarian Forests, W Bohemian Massif	Variscan granites, redwitzites, intermediate granitoids	334-312		late to post-orogenic granitoid formation during Late Visean metamorphism and anatexis	0.282603	0.282423	0.75	− 5.6	Siebel and Chen (2010)
Bavarain Forest, W Bohemian Massif	migmatite	342-330, 333-320	426-420	granulite-facies metamorphism, late-Variscan anatectic overprint					Siebel et al. (2012)
South/central part									
S Bohemian Batholith	Weinsberg type granites	331-323		magma emplacement					Gerdes et al. (2003)
Southeast part									
Varied group	Dobra gneiss	1377±10		protolith emplacement of the Dobra gneiss					Gebauer and Friedl (1994)
Varied and Monotonous Groups	metasediments	672±57 to 2281±22		early Proterozoic crust formation event (from 2.0 to 2.2 Ga)					Kröner et al. (1988)
Rastenberg batholith	granodiorite	353±9, 338±2	623±22, >1206	first magma formation during Variscan plutonism, granodioritic magma intrusion into the middle crust					Klötzli and Parrish (1996)
S Bohemian Massif (S Bohemian Batholith, Gföhl nappe, Drosendorf nappe)	pre-Variscan granitoids (orthogneiss, granulite, granite)	585-565, 488±6, 445±10		Cadomian and Ordovician magmatism					Friedl et al. (2004)
Dunkelsteiner Wald, S Bohemian Massif	granulite	342±3 and 337±2.7	460-390	Variscan regional metamorphism, exhumation into mid-crustal levels					Friedl et al. (2011)
Montonous Unit	gneiss	550, 470	2650, 2350, 2100-1700, 850						Kosler et al. (2014)

Varied Unit	gneiss	550-470, 340-320	2500-2400, 2100-1650, 1300-1050		Kosler et al. (2014)
Gföhl Unit	gneiss	580, 470, 340			Kosler et al. (2014)
Eastern Alps					
Tauern Window	amphibolite, hornblendite, metagabbro	657±15, 539±10, 496-350, 314-301		Variscan metamorphism, Cambro-Ordovician magmatism, calc-alkaline magmatism (Pan-African event)	von Quadt (1992)
Ötztal	Winnebach migmatite	490±9		migmatization	Klötzli-Chowanetz et al. (1997)
middle Tauern Window	dacitic dike, gneiss, amphibolite	547±27, 529±18, 519±14, 340±5	~640, 581±28	orthogneiss precursor (I-type granite) emplacement, Variscan dike intrusion	Eichhorn et al. (1999)
central Tauern Window	leucocratic orthogneisses	374±10, 343±6 to 340±4, 300±5 to 296±4, 279±9 to 271±4		Visean, Gzhelian and Early Permian pulses of magmatism	Eichhorn et al. (2000)
Habach terrane, Tauern Window	amphibolite, hornblende plagioclase gneiss	551±9, 482±5		protolith formation	Eichhorn et al. (2001)
SW Tauern Window	mafic-ultramafic cumulates, metagraniodiorite	309±5, 295±3		Late Carboniferous calc-alkaline plutonic activity, emplacement of granodiritic to tonalitic intrusions	Cesare et al. (2002)
central Tauern Window	metagabbro, amphibolite, biotite schist, gneiss	368±17, 362±6, 351-343, 334±16		Variscan basic magmatism, maximum sedimentation ages	Kebede et al. (2005)
Eclogite Zone, Tauern Window	jadeite-gneiss	466±2, 437±2, 288±9	691-503	Ordovician magmatism, Late Carboniferous to early Permian magmatic event	Miller et al. (2007)
W Tauern Window	granite gneiss, rhyolite, granodiorite	335±1.5, 310±1.5, 304±3, 292±2, 280±5		Visean and Westfalian–Stefanian magmatism, Lower Permian magma emplacement	Veselá et al. (2011)
Austroalpine basement (south of the Tauern Window)	metagranite, eclogitic amphibolite, metarhyolite	477±4 to 470±3		Early Ordovician magmatism	Siegesmund et al. (2007)
Carnic Alps	sandstone	650±12, 530±53 to 518±38	2085±11, 1964±23, 1439±37, 876±70	acidic magmatism (Late Cadomian tectonic events)	Neubauer et al. (2001)
eastern Greywacke Zone	orthogneiss boulde, paragneiss, aplite	514, 502-498, ~391	~2545	Late Cambrian/Early Ordovician thermal overprint and magmatism, Devonian metamorphism	Neubauer et al. (2002)

Table S1
Click here to download Electronic Supplementary Material: renamed_a1969.pdf

Table S2

Table S3

Click here to download Electronic Supplementary Material: renamed_5d6f1.xls

Table S4
Click here to download Electronic Supplementary Material: renamed_9f98c.xls

Table S5